Regulation of caveolin-1 membrane trafficking by the Na/K-ATPase

Ting Cai,[1] Haojie Wang,[2] Yiliang Chen,[1] Lijun Liu,[1] William T Gunning,[3] Luis Eduardo M. Quintas,[4] and Zi-Jian Xie[1,2]

[1]Department of Physiology and Pharmacology, [2]Department of Medicine, and [3]Department of Pathology, University of Toledo College of Medicine, Health Science Campus, Toledo, OH 43614
[4]Departamento de Farmacologia Básica e Clínica, Instituto de Ciências Biomédicas, Universidade Federal do Rio de Janeiro, Cidade Universitária, 21941-902, Rio de Janeiro, Brasil

Here, we show that the Na/K-ATPase interacts with caveolin-1 (Cav1) and regulates Cav1 trafficking. Graded knockdown of Na/K-ATPase decreases the plasma membrane pool of Cav1, which results in a significant reduction in the number of caveolae on the cell surface. These effects are independent of the pumping function of Na/K-ATPase, and instead depend on interaction between Na/K-ATPase and Cav1 mediated by an N-terminal caveolin-binding motif within the ATPase α1 subunit. Moreover, knockdown of the Na/K-ATPase increases basal levels of active Src and stimulates endocytosis of Cav1 from the plasma membrane. Microtubule-dependent long-range directional trafficking in Na/K-ATPase–depleted cells results in perinuclear accumulation of Cav1-positive vesicles. Finally, Na/K-ATPase knockdown has no effect on processing or exit of Cav1 from the Golgi. Thus, the Na/K-ATPase regulates Cav1 endocytic trafficking and stabilizes the Cav1 plasma membrane pool.

Introduction

The Na/K-ATPase, also known as the sodium pump, is a ubiquitous trans-membrane enzyme that transports Na^+ and K^+ across the plasma membrane by hydrolyzing ATP (Sweadner, 1989; Lingrel and Kuntzweiler, 1994; Kaplan, 2002). Interestingly, cells appear to contain two functionally separable pools of Na/K-ATPase, and a majority of the cellular Na/K-ATPase is engaged in cellular activities other than pumping ions (Liang et al., 2007). Moreover, the nonpumping Na/K-ATPase apparently resides in caveolae and interacts directly with multiple proteins including protein kinases, ion transporters, and structural proteins to exert its nonpumping functions. For example, the interaction between Na/K-ATPase and Src controls basal Src activity (Tian et al., 2006). It also forms a functional receptor complex for cardiotonic steroids such as ouabain to stimulate tyrosine phosphorylation of several downstream effectors including caveolin-1 (Cav1) (Yuan et al., 2005; Tian et al., 2006; Nguyen et al., 2007). Furthermore, the caveolar Na/K-ATPase appears to be an important scaffold that is capable of assembling both signaling and structural protein complexes. For instance, the interaction between the Na/K-ATPase and IP3 receptors is important for the junctional Ca^{2+} signaling in many cell types (Aizman et al., 2001; Yuan et al., 2005; Chen et al., 2007; Edwards and Pallone, 2007), and the Na/K-ATPase is essential for the integrity of tight junctions in epithelial cells (Rajasekaran et al., 2005).

There are three genes and six isoforms of caveolin (Williams and Lisanti, 2004). Cav1 is a 22-kD protein and is expressed in endothelial, epithelial, and other cells. It has a 33-residue central hydrophobic region and is palmitoylated on multiple cysteine residues. Cav1 is considered as an integral membrane protein, and both the hydrophobic region and palmitoylation are important for targeting Cav1 to the plasma membrane. Cav1 was originally found as a novel tyrosine kinase substrate in Rous sarcoma transformed cells (Glenney, 1989). It has now been investigated as the biochemical marker and structural protein of caveolae in most types of cells (Rothberg et al., 1992; Anderson, 1998). Caveolae are flask-shaped vesicular invaginations of plasma membrane and are enriched in cholesterol, glycosphingolipids, and sphingomyelin (Anderson, 1998; Razani et al., 2002). The current interests in caveolin and caveolae are derived from their multiple functions in dynamic cellular processes such as signal transduction and endocytosis (Balasubramanian

Correspondence to Zi-Jian Xie: zi-jian.xie@utoledo.edu

Abbreviations used in this paper: Cav1, caveolin-1; CBM, caveolin-binding motif; FRET, fluorescence resonance energy transfer; mCBM, mutated caveolin-binding motif; MSD, mean square displacement.

The online version of this article contains supplemental material.

The Rockefeller University Press $30.00
J. Cell Biol. Vol. 182 No. 6 1153–1169
www.jcb.org/cgi/doi/10.1083/jcb.200712022

et al., 2007; Parton and Simons, 2007; Salanueva et al., 2007). Moreover, defects in caveolin trafficking are associated with human diseases and pathological conditions (Schlegel et al., 2000; Pol et al., 2005; Parton and Simons, 2007)

Although early studies suggest that caveolae might form at the plasma membrane when a sufficient amount of Cav1 is delivered, more recent studies using GFP-tagged Cav1 demonstrate that caveolar vesicles are actually formed in the Golgi complex and that these preassembled caveolar vesicles can undergo continuous cycles of fusion and fission with the preexisting caveolae in the plasma membrane (Pelkmans and Zerial, 2005; Tagawa et al., 2005). Several regulatory mechanisms have been identified to regulate these dynamic processes. For example, removal of cholesterol or activation of Src family kinases is known to increase the fission of caveolar vesicles, whereas Src knockout stabilizes plasma membrane caveolae (Pelkmans and Zerial, 2005; Le Lay et al., 2006). Moreover, the plasma membrane Cav1 is highly immobile unless cells are exposed to either chemical or viral stimuli (Pelkmans et al., 2001; Thomsen et al., 2002). It is known that caveolins interact with multiple membrane proteins via their scaffolding domain. These interactions appear to be important for "trapping" receptors in the caveolae to form efficient signaling microdomains (Couet et al., 1997; Liu et al., 2002). Because the Na/K-ATPase is an abundant caveolar resident in the plasma membrane and regulates basal cellular Src activity, we postulated that the Na/K-ATPase might interact with Cav1 and regulate its membrane trafficking. To test this hypothesis, we determined whether changes in plasma membrane Na/K-ATPase amount and structure affected Cav1 distribution and mobility in LLC-PK1 cells. Our new findings showed that the Na/K-ATPase regulates the membrane trafficking of Cav1.

Results

The Na/K-ATPase knockdown changes subcellular distribution of Cav1

Recently, we have found that there are two functionally separable pools of Na/K-ATPase in LLC-PK1 cells (Liang et al., 2006, 2007). Graded knockdown of Na/K-ATPase by the expression of an α1-specific siRNA preferentially abolishes the pool of nonpumping Na/K-ATPase that resides in caveolae and interacts with Cav1 (Liu et al., 2003; Wang et al., 2004; Liu et al., 2005; Liang et al., 2007). To investigate whether changes in the amount of caveolar Na/K-ATPase affect cellular Cav1 distribution, we used a well-established detergent-free and carbonate-based density gradient fractionation procedure (Song et al., 1996; Liu et al., 2003) and prepared caveolar fractions from the control LLC-PK1 cells (P-11) and Na/K-ATPase knockdown cell lines (A4-11 and TCN23-19). Western blot analysis of total cell lysates showed that A4-11 cells had ∼44% of the α1 subunit in comparison to the control P-11 cells, whereas TCN23-19 cells contained ∼10% of the α1 subunit (Fig. 1 A; Liang et al., 2006). When different fractions were analyzed, we found that both Cav1 and the α1 were concentrated in fraction 4/5 in control P-11 cells (Fig. 1 B), which is in agreement with what has been reported (Liu et al., 2003; Wang et al., 2004). However, this pattern of distribution was significantly altered in the knockdown cells. Overall, knockdown of the Na/K-ATPase redistributed Cav1 from the fraction 4/5 to high density fractions that contain protein markers for ER (calnexin), Golgi (GM130), early endosomes (EEA-1) (Fig. 1 C), and other subcellular structures (Liu and Askari, 2006; Mayoral et al., 2007). Quantitatively, although no significant change in total cellular Cav1 content was detected in A4-11 cells, a 22 ± 4% decrease was observed in TCN23-19 cells (Fig.1 D). When the ratio of fraction 4/5 Cav1 versus total was calculated, we found that the changes in Cav1 distribution appeared to be correlated with the amount of α1 in different cell lines. Although 47 ± 8% (n = 5) of Cav1 was detected in fraction 4/5 in control P-11 cells, only 22 ± 3% (n = 3) and 12 ± 2% (n = 4) of Cav1 were found in this fraction in A4-11 and TCN23-19 cells, respectively (Fig. 1 D). These results implied that decreases in the Na/K-ATPase might redistribute Cav1 from the low density caveolae into high density subcellular organelles such as endosomes.

The Na/K-ATPase knockdown alters the plasma membrane distribution of endogenous as well as YFP-tagged Cav1

To confirm the above findings, we performed the immunostaining assay to visualize the endogenous Cav1 distribution in fixed cells. As depicted in Fig. 2 A, Cav1 resided in the plasma membrane in control P-11 cells. Using a semi-quantitative analysis detailed in Materials and methods, we estimated that the plasma membrane pool contained 56 ± 2% (n = 32 cells) of total cellular Cav1 signal. In agreement with prior observations, we also detected perinuclear distribution of Cav1, most likely due to the slow transport of Cav1 through the Golgi network (Luetterforst et al., 1999; Nichols, 2003; Pol et al., 2005). In contrast to the control P-11 cells, the plasma membrane distribution of Cav1 in TCN23-19 cells was significantly reduced (26 ± 1%, n = 49 cells, $P < 0.01$ in comparison with that in P-11 cells) with a concomitant accumulation of Cav1-positive vesicles in the perinuclear region as well as in the cytoplasm (Fig. 2 A).

To further study the cellular distribution of Cav1 in live cells, we constructed the plasmids expressing EYFP-fused to either the N terminus (YFP-Cav1) or C terminus (Cav1-YFP) of Cav1. It has been demonstrated that both N- and C-tagged caveolin proteins had a similar overall distribution when they were transfected into cultured cells. However, different terminal tag did affect the functionality of Cav1 (Pelkmans et al., 2001). Thus, we studied both fusion proteins in our control and Na/K-ATPase knockdown cells. As shown in Fig. 2 B, 24 h after transfection, a large portion of Cav1-YFP fusion protein was already transported to the plasma membrane in control P-11 cells (58 ± 2%, n = 41 cells). As expected (Luetterforst et al., 1999; Nichols, 2003; Pol et al., 2005), a small amount of the expressed fusion protein resided in the perinuclear region, and the cytoplasm contained a few Cav1-YFP–positive vesicles. In contrast, a vast majority of the fusion protein was found in vesicles with much less signal being detected in the plasma membrane in TCN23-19 cells (32 ± 1%, n = 40 cells, $P < 0.01$ in comparison with that in P-11 cells) (Fig. 2 B). This is consistent with the findings presented in Fig. 2 A. Moreover, these

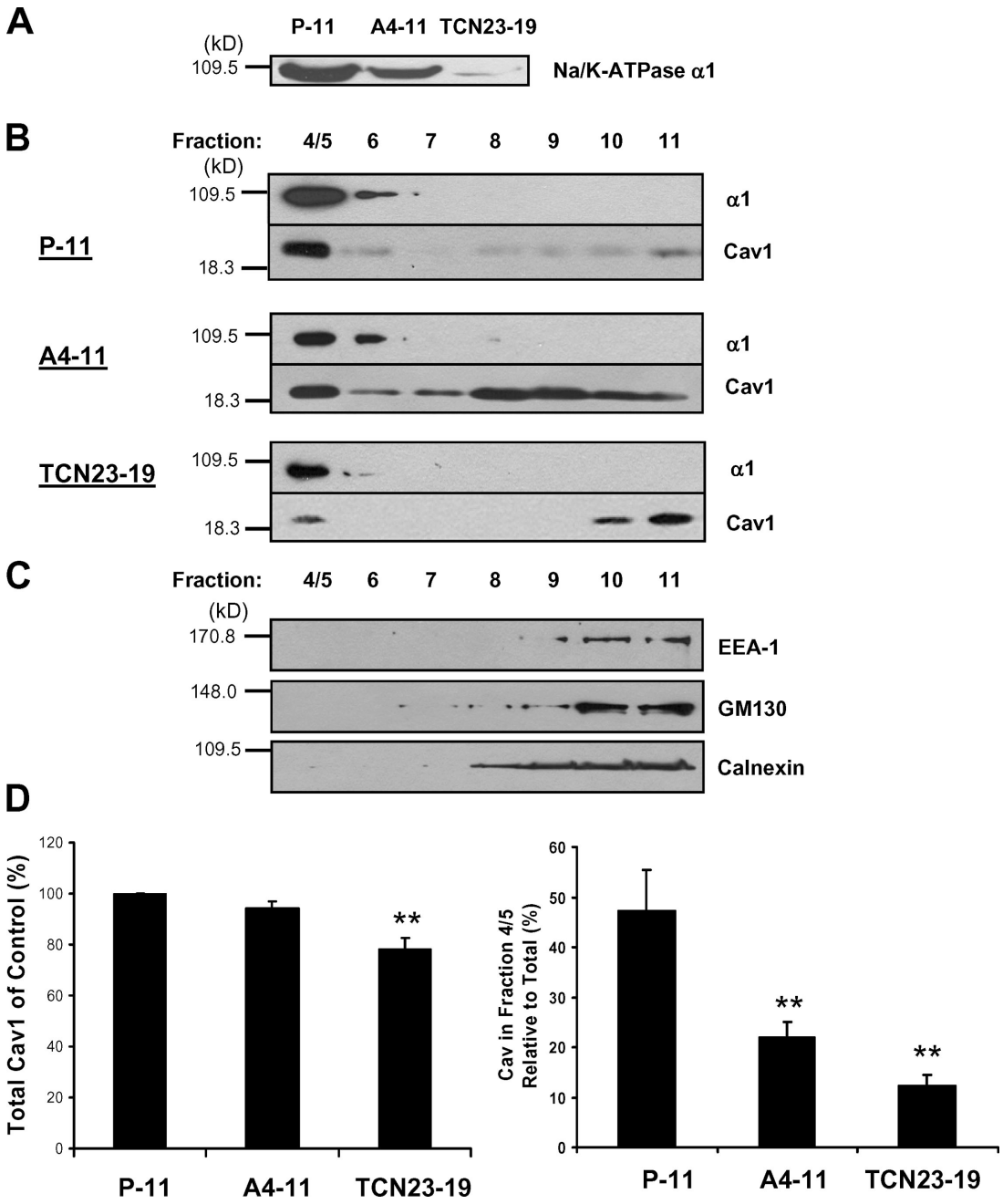

Figure 1. **Na/K-ATPase knockdown changes subcellular distribution of Cav1.** (A) A representative Western blot shows the amount of α1 in total cell lysates from different cell lines. (B) Total cell homogenate from control (P-11) and knockdown (A4-11 and TCN23-19) cells was fractionated by gradient centrifugation as described under Materials and methods. Fractions (1 ml each) were collected from top to bottom, and equal volume of each fraction was immunoblotted for proteins as indicated. (C) Distribution of different subcellular markers in different fractions: EEA-1 (early endosomes), GM130 (Golgi), Calnexin (ER). A representative blot from P-11 cells is shown. Similar distribution of these markers was detected in the knockdown cells. (D) Cav1 in total cell lysates and fraction 4/5 was analyzed by Western blot. Quantitative data (mean ± SE) from 4–6 independent experiments are shown, **, $P < 0.01$ in comparison to control.

Cav1-YFP–positive vesicles were much larger in size in comparison with those detected in the control P-11 cells, and resided in the perinuclear region as well as scattered in the cytoplasm. When the same experiment was repeated in cells transfected with YFP-Cav1, a similar but more severe alteration was found in TCN23-19 cells (Fig. 2 B). Together, these findings were consistent with the data presented in Fig. 1, and indicated that knockdown of the Na/K-ATPase reduced the amount of Cav1 in the plasma membrane and concomitantly increased Cav1-positive vesicles in the cytoplasm.

The Na/K-ATPase knockdown affects caveolae formation

Cav1 is the major structural component of caveolae. To determine the effect of Na/K-ATPase knockdown on caveolae formation, we processed both P-11 and TCN23-19 cells for ultrastructural analysis.

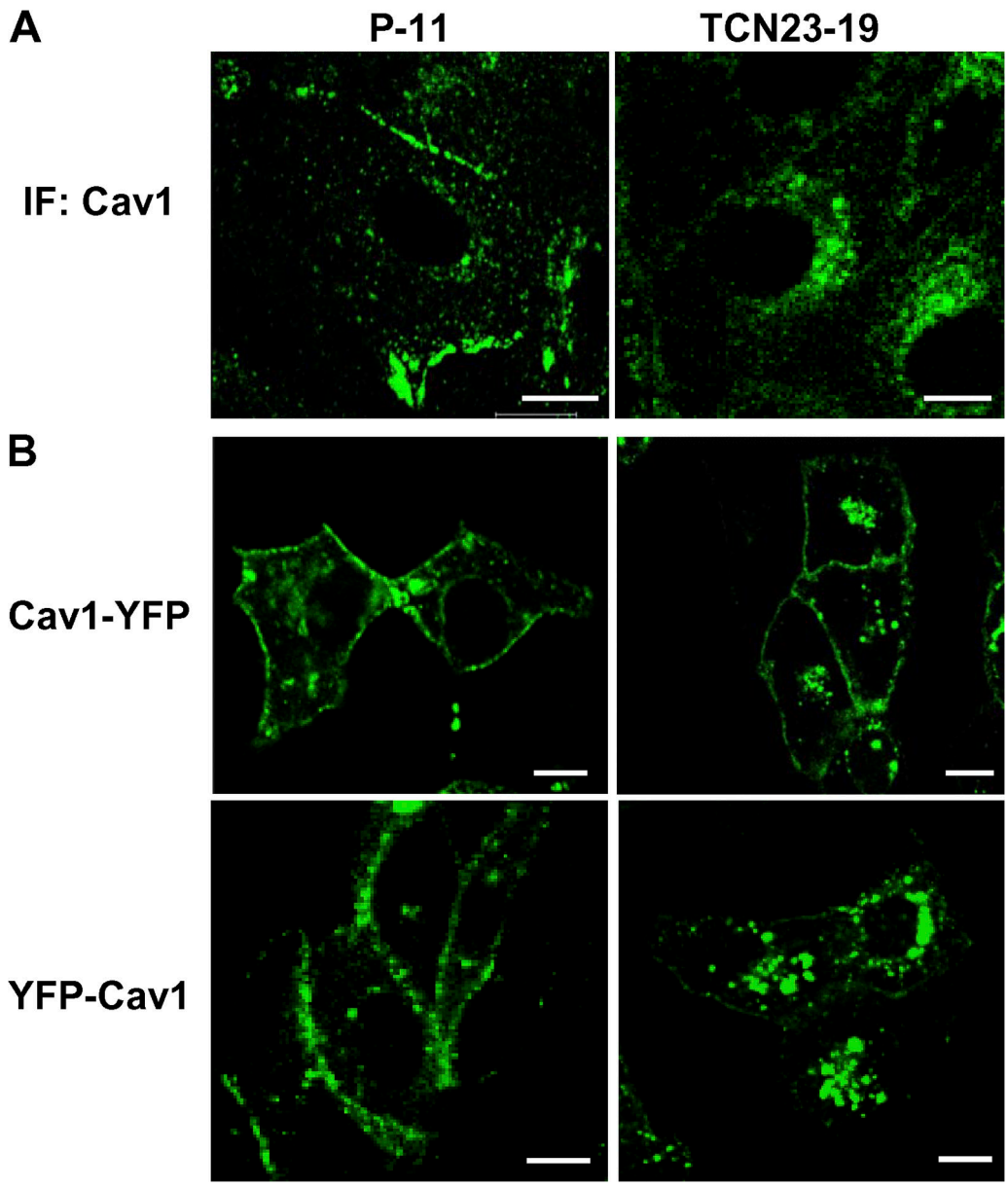

Figure 2. **Effects of Na/K-ATPase knockdown on cellular distribution of Cav1.** (A) P-11 and TCN23-19 cells were fixed, permeabilized, and stained for total cellular Cav1. (B) Cells were transfected with either YFP-Cav1 or Cav1-YFP and analyzed after 24 h. Representative images of five independent experiments are shown. Bar, 5 µm.

The typical caveolae appear as rounded plasma membrane invaginations of 50–80 nm in diameter in endothelial cells and adipocytes (Richter et al., 2008), whereas the caveolae found in epithelial cells are on average a bit smaller (Pelkmans and Helenius, 2002). In accordance, caveolae with a diameter between 30–80 nm were readily detectable on the surface in P-11 (Fig. 3 A, insets b and c) but not TCN23-19 cells (Fig. 3 C). Coated pits were also evident in some images (see Fig. 3 A, inset a). Quantitatively, we detected 0.47 ± 0.01 surface connected caveolae per µm of the plasma membrane in control P-11 cells. In TCN23-19 cells, this number decreased to 0.08 ± 0.04, an 82% reduction (Fig. 3). Consistently, when immuno-EM was performed, we found that ∼65 ± 7% of surface gold were in clusters, surrounding 30–80-nm vesicles close to or clearly connected to the plasma membrane in P-11 cells (Fig. 3 B). In contrast, only 15 ± 6% of surface gold particles were found located in surface caveolar structures in TCN23-19 cells (Fig. 3 D). These findings, together with those depicted in Fig. 2, indicate that the Na/K-ATPase knockdown reduced the number of caveolae. Interestingly, unlike knockdown of Cavin (Hill et al., 2008), the Na/K-ATPase knockdown also caused a redistribution of Cav1 from the plasma membrane to cytosolic compartments.

The Na/K-ATPase interacts with Cav1 via its N-terminal caveolin-binding motif

We have shown that the Na/K-ATPase can be coimmunoprecipitated with Cav1 and that the purified Na/K-ATPase binds to

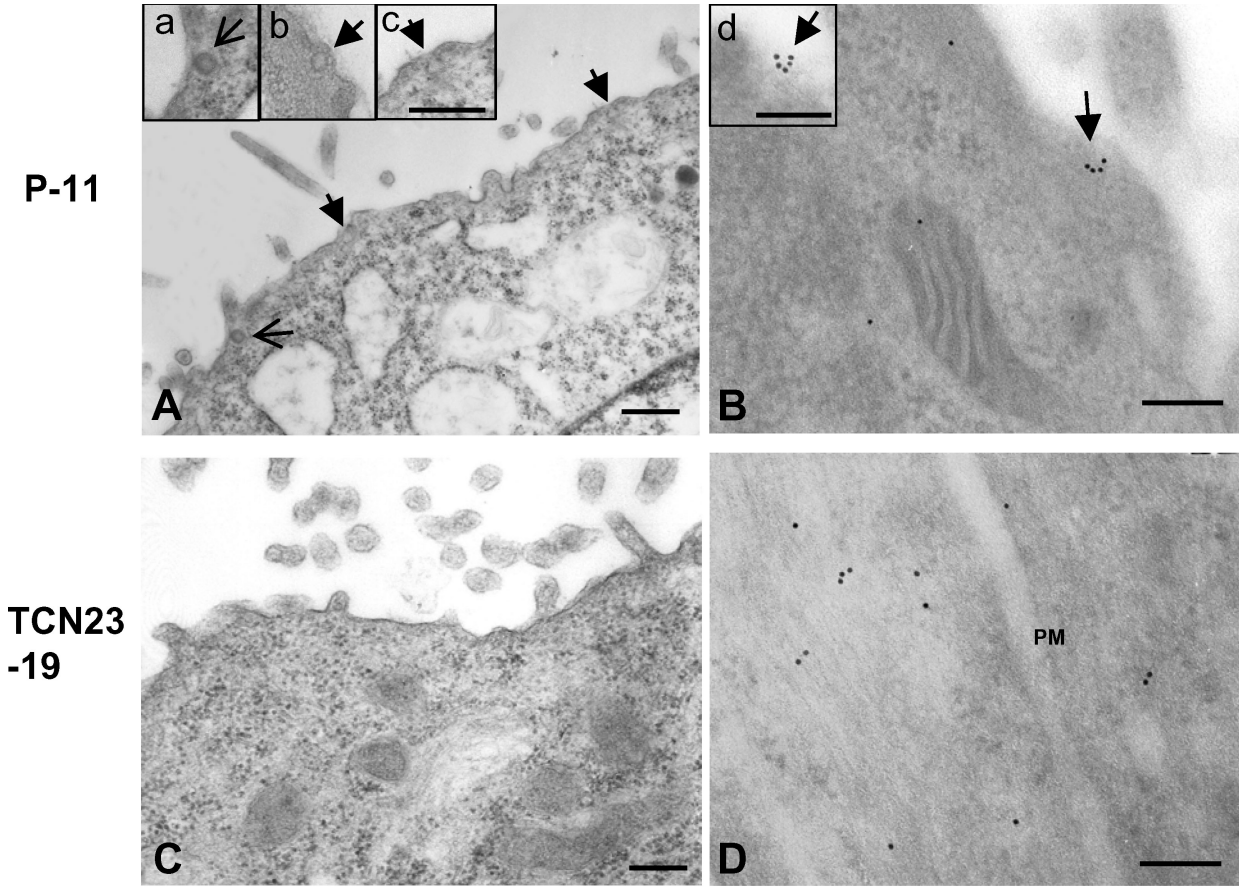

	P-11	TCN23-19
Average number of caveolae close to or clearly connected to PM per μm	0.47 ± 0.01	0.08 ± 0.004
Percentage of surface gold related to caveolae structures close to or clearly connected to PM	65 ± 7%	15 ± 6%

Figure 3. **Effects of Na/K-ATPase knockdown on caveolae formation.** Control or Na/K-ATPase knockdown cells were fixed and embedded, and ultrathin sections were analyzed by electron microscopy. Left: caveolae (A and insets b and c) were detected in the control cells as pointed by solid arrow, but rarely seen in the knockdown cells (C). Right: immuno-EM was performed to examine the localization of Cav1. Surface clusters of gold particles were detected in P-11 (B and inset d), but rarely seen in TCN23-19 cells (D). The number of caveolae or gold particles in each cell line was determined in images randomly acquired at the same magnification. Quantitative data were obtained by double-blind analysis in over 40 cells from each cell line, and listed in the table. A coated pit is pointed by an open arrow in A and inset "a". Representative images are shown. Bar, 200 nm.

GST-Cav1 N terminus (Wang et al., 2004). To determine whether the interaction between Na/K-ATPase and Cav1 plays a role in regulating caveolar vesicle trafficking, we first performed fluorescence resonance energy transfer (FRET) analysis to test whether these two proteins have the potential to directly interact in live cells. YFP-α1 was used because our prior experiments showed that it could be expressed and targeted to the plasma membrane as the endogenous α1 (Tian et al., 2006). To test which Cav1 construct could be used for FRET analysis, we first transfected the TCN23-19 cells with either CFP-Cav1/YFP-α1 or Cav1-CFP/YFP-α1, then measured the FRET efficiency. As depicted in Fig. 4 A, both CFP-Cav1 and YFP-α1 were targeted to the plasma membrane. When the plasma membrane signals were analyzed, we found significant FRET between this pair of proteins (Fig. 4, A and B), indicating that the Na/K-ATPase and Cav1 are likely to interact in the plasma membrane. When the same experiment was repeated with Cav1-CFP and YFP-α1, we found that both were also targeted to the plasma membrane (not depicted) and yielded a significant FRET. However, CFP-Cav1/YFP-α1 yielded a higher FRET efficiency than that of Cav1-CFP/YFP-α1 pair (15.5 ± 3.4% vs. 9.2 ± 1.3%, $n = 5$, $P < 0.05$). This finding is consistent with the fact that the scaffolding domain and a putative caveolin-binding motif are located at the N termini of both proteins (see next paragraph). Thus, the

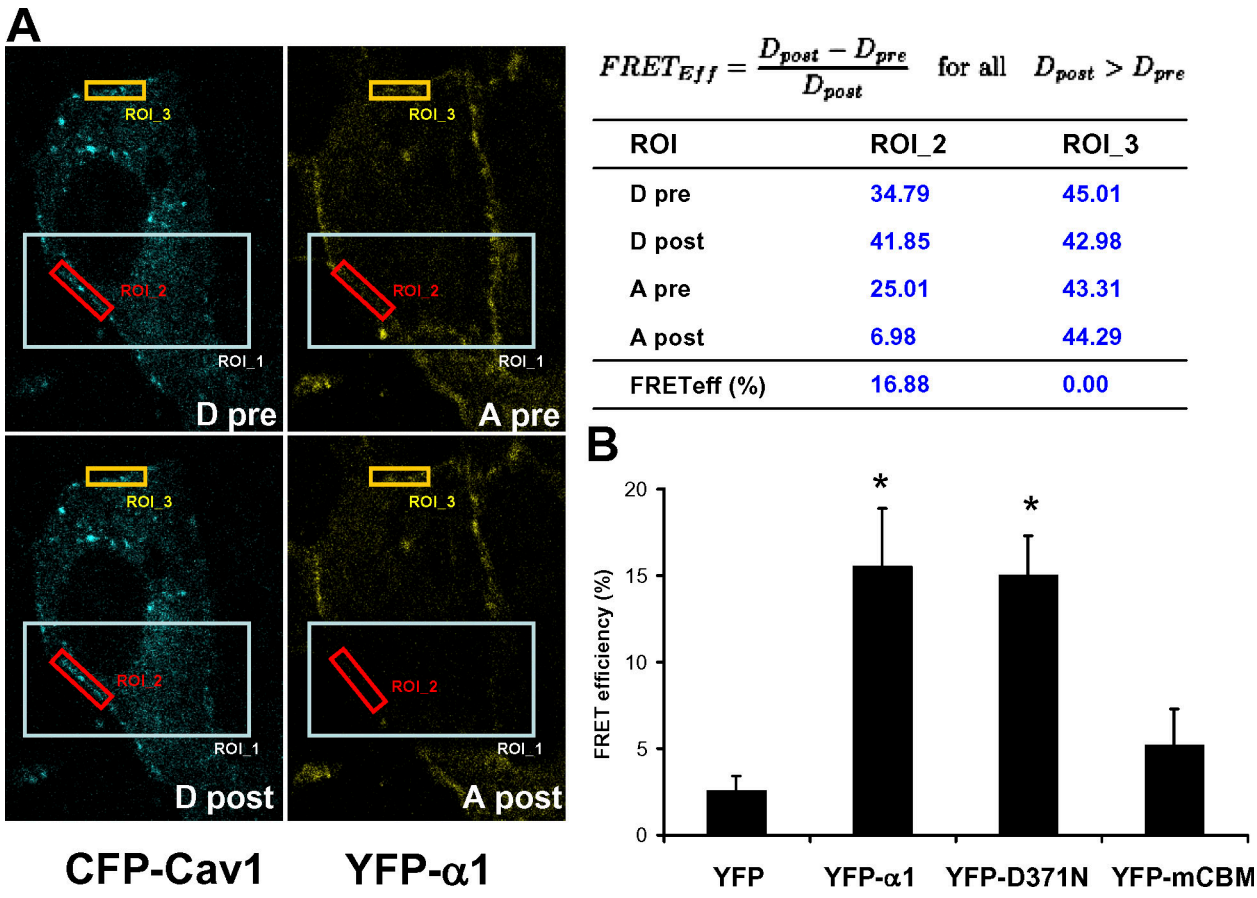

Figure 4. **FRET analyses of the interaction between Cav1 and Na/K-ATPase α1 subunit.** YFP- tagged α1, D371N, or mCBM was transfected together with CFP-Cav1 into TCN23-19 cells. FRET analyses were done as described in Materials and methods. YFP-only and CFP-Cav1–transfected cells were used as a negative control. (A) Images were taken before and after photobleaching. The ROI_1 was bleached at 515 nm with full power. Small regions of plasma membrane in (ROI_2) and out (ROI_3) of the bleached area were selected for measurement, and FRET efficiency was calculated from the measurements using the equation as shown in the table. Bar, 2 µm. (B) Corrected FRET efficiency was calculated from each experiment and values are mean ± SE of 4–5 independent experiments. *, $P < 0.05$ in comparison to control.

detected difference in FRET efficiency between the N- and C-terminal tags of Cav1 provides a nice control for validating the FRET analysis. Therefore, the following FRET analyses were conducted with the CFP-Cav1/YFP-α1 pair.

To test whether the interaction requires the pumping function of Na/K-ATPase, we performed FRET analysis between a pump-null mutant of YFP-α1 (D371N) and CFP-Cav1. Both proteins were targeted to the plasma membrane and the D371N mutant was capable of interacting with Cav1 to generate FRET efficiency of 15.0 ± 2.3% in the plasma membrane (Fig. 4 B).

Sequence analysis revealed that the α1 subunit of Na/K-ATPase contains two highly conserved potential caveolin-binding motifs (CBM), one being at the N terminus and the other at the C terminus (Wang et al., 2004). To test whether these potential α1 CBMs are involved in the interaction, we focused on the N-terminal CBM because the C-terminal CBM resides extracellularly according to the newly released 3D structure of the Na/K-ATPase (Morth et al., 2007). Using a strategy developed by others (Leclerc et al., 2002; Wang et al., 2002; Brazer et al., 2003; Sato et al., 2004), we mutated two of the aromatic amino acid residues in the CBM to Ala (F97A and F100A). Imaging analysis showed that the mutated α1 (mCBM) was targeted to the plasma membrane as wild-type α1. However, it failed to generate significant FRET with Cav1 (Fig. 4 B). These findings indicate that the plasma membrane Na/K-ATPase is likely to interact with Cav1 directly in live cells via the α1 N-terminal CBM.

Wild-type α1 and the pump-null D371N mutant, but not the mCBM, rescued Cav1 subcellular localization

To functionally assess the role of the interaction between Na/K-ATPase and Cav1 in regulating cellular distribution of Cav1, we rescued TCN23-19 cells by expressing a wild-type rat α1. After the stable cell lines were established, we repeated the density fractionation assays. As shown in Fig. 5, expression of a wild-type rat α1 in TCN23-19 cells not only restored cellular Na/K-ATPase activity (Liang et al., 2006), but was also able to target Cav1 into fraction 4/5 as in the control P-11 cells (Fig. 5 B). To be sure that this restoration is not a cell-specific phenomenon, we repeated the same experiments in PY-17 cells, another Na/K-ATPase knockdown cell line (Liang et al., 2006), showing that expression of a rat α1 was indeed sufficient to restore Cav1 targeting to the fraction 4/5 in this cell line (see Fig. S1, available

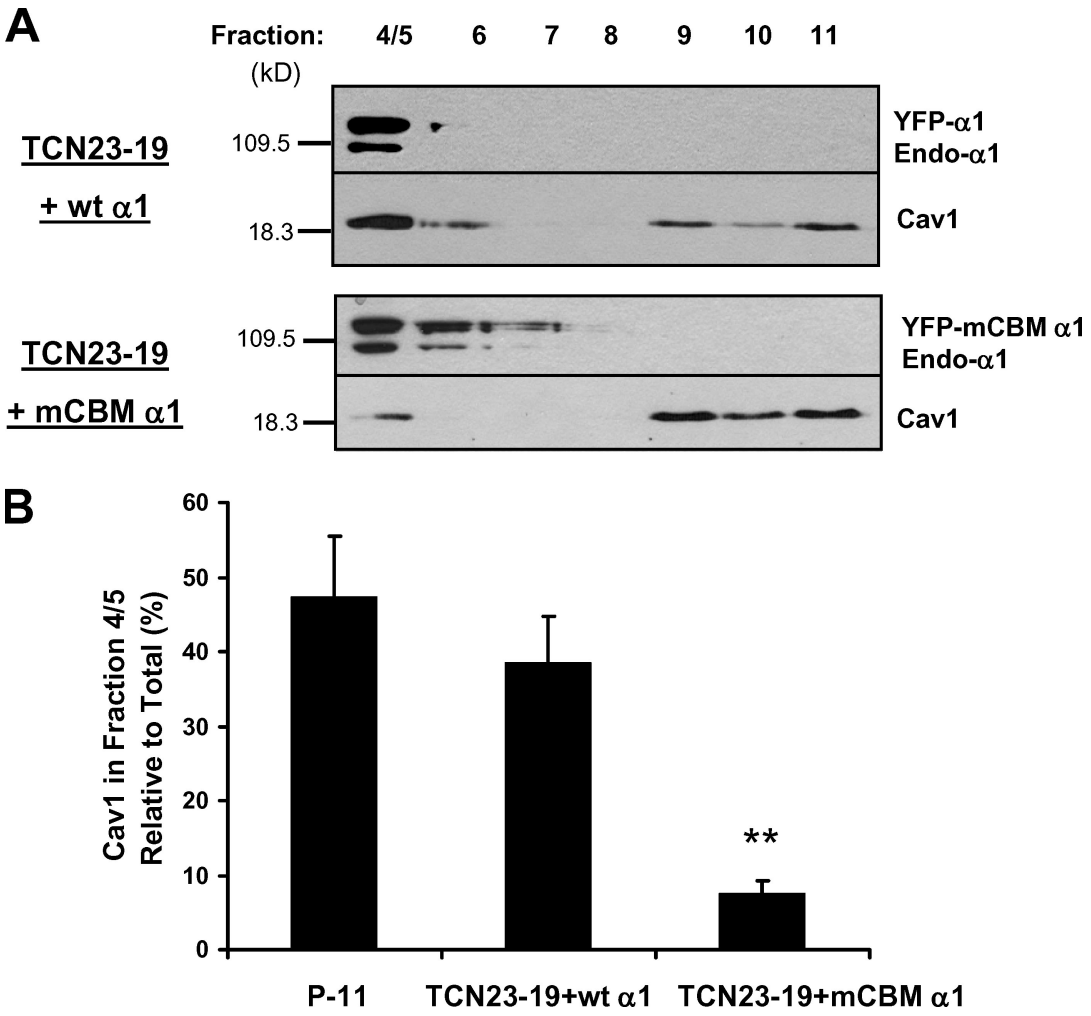

Figure 5. **Knocking-in a wild-type, but not mCBM α1 mutant rescues Cav1 distribution in TCN23-19 cells.** TCN23-19 cells were rescued by YFP-tagged wild-type α1 (wt α1) or mCBM. Stable cell lines were generated and analyzed as described in Fig. 1. (A) A set of representative Western blots from four independent experiments showing the expression of both YFP-α1/mCBM α1 (140 kD) and residual endogenous α1 (110 kD), and the distribution of Cav1 in each fraction. (B) Combined data from four different experiments shows that expression of wild-type rat α1, but not the mCBM α1, restored the distribution of Cav1 into the 4/5 fraction in TCN23-19 cells . **, $P < 0.01$ in comparison with control P-11. Endo α1: endogenous α1.

at http://www.jcb.org/cgi/content/full/jcb.200712022/DC1). In contrast, rescuing TCN23-19 cells with the mCBM α1 only restored the cellular Na/K-ATPase, but failed to change Cav1 distribution because most of Cav1 remained in the heavy fractions (Fig. 5). These findings are consistent with the notion that the interaction between Na/K-ATPase and Cav1 is important for trafficking Cav1 to the plasma membrane.

To seek further evidence to support the above conclusion, we repeated the transient transfection and imaging analyses using different α1 constructs. As shown in Fig. 6 A, in TCN23-19 cells rescued by wild-type α1 (pointed by red arrowhead), the expressed Cav1-CFP was targeted to the plasma membrane. On the other hand, in the same image we found that Cav1-CFP–positive vesicles were largely retained in the cytoplasm in a cell that did not express a significant amount of YFP-α1 (pointed by blue arrowhead). Moreover, expression of the YFP-mCBM α1 mutant failed to restore the cellular distribution of Cav1-CFP (Fig. 6 C), which is consistent with the fractionation studies presented in Fig. 5.

Because the YFP-mCBM α1 mutant can form an active pump, the above findings indicate that the effect of Na/K-ATPase on Cav1 distribution is unlikely due to decreases in pumping activity or subsequent changes in intracellular ion concentration. To seek further support to this contention, we rescued TCN23-19 cells with a pump-null D371N mutant. As shown in Fig. 6 B, expression of the YFP-D371N mutant was able to restore normal cellular distribution of Cav1-CFP.

Cav1 can exit from the Golgi complex in Na/K-ATPase knockdown cells

The decrease in plasma membrane Cav1 in TCN23-19 cells could be due to defects in the Golgi processing of Cav1. To test whether the Golgi exit of Cav1 in the knockdown cells is significantly reduced, we first determined whether perinuclear Cav1-YFP colocalized with giantin, a trans-Golgi marker, and calnexin, an ER marker. As expected, some colocalization between Cav1-YFP and giantin (Fig. 7, A and B), but very few between Cav1-YFP and calnexin (not depicted), was detected. However, a

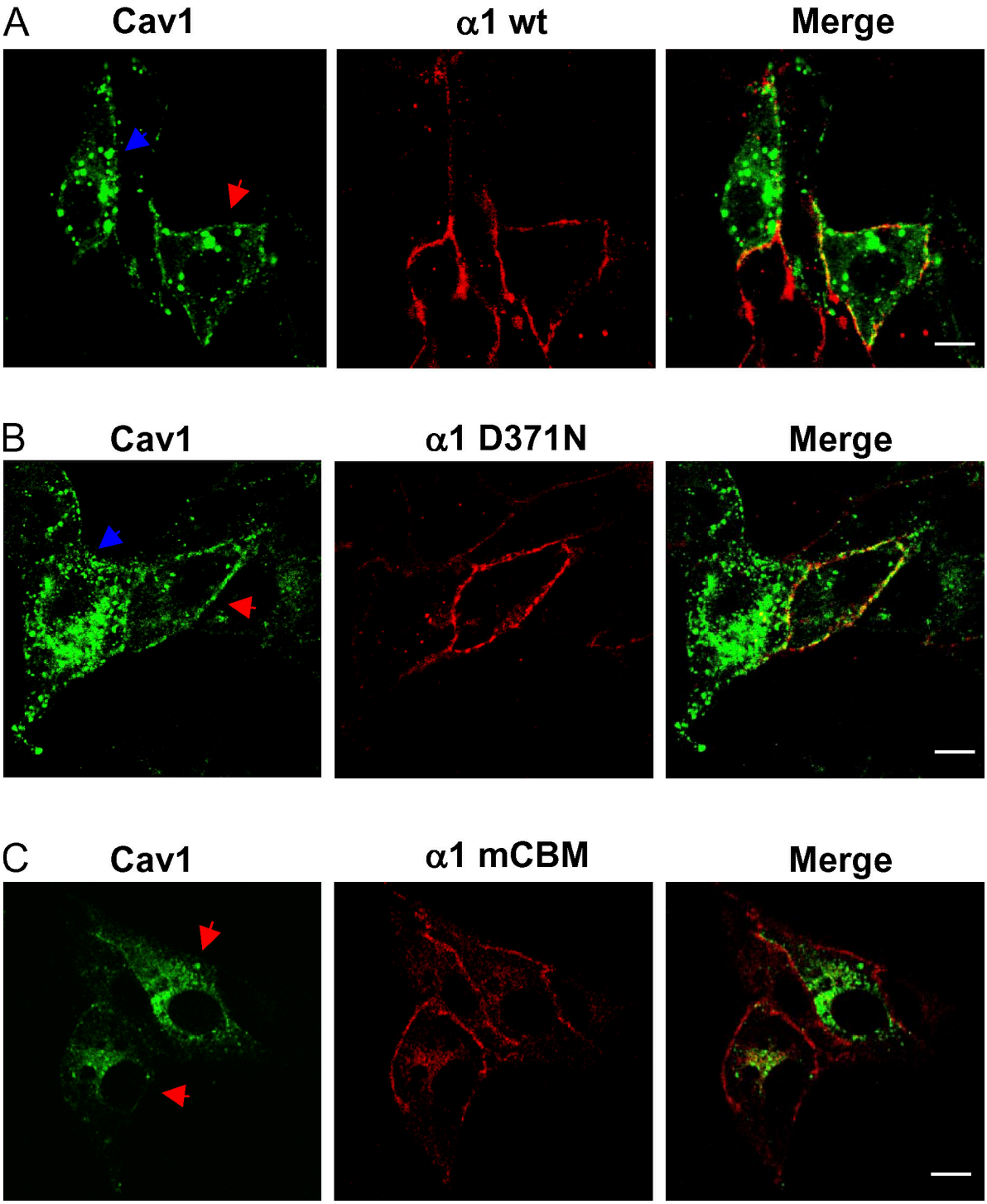

Figure 6. **Expression of wild-type rat α1 and D371N, but not mCBM, in TCN23-19 cells restored Cav1 distribution.** Cells were cotransfected with caveolin-CFP and YFP-tagged wild-type rat α1 (α1 wt), D371N, or mCBM. Images were taken by confocal microscope, and pseudo-color was assigned to the images to show colocalization. Red arrowhead: rescued cells; blue arrowhead: cells that were not rescued by either rat α1 or its mutants. A set of representative images of three separate experiments is shown. Bar, 5 μm.

majority of the accumulated perinuclear Cav1-YFP in the knockdown cells apparently resided in vesicles outside of the Golgi complex (Fig. 7 B). This pattern of distribution was also true in YFP-Cav1–expressing cells (not depicted). To rule out the possibility that the different cell lines may make a difference in processing transfected proteins, we then performed the second set of experiments in which we examined the Golgi distribution of endogenous Cav1, showing essentially the same pattern of Cav1 distribution in both types of cells (Fig. 7, C and D). Moreover, it is known that the Golgi pool of caveolin is in low molecular weight oligomers and is soluble in low concentration of Triton X-100 at low temperature (Pol et al., 2005).

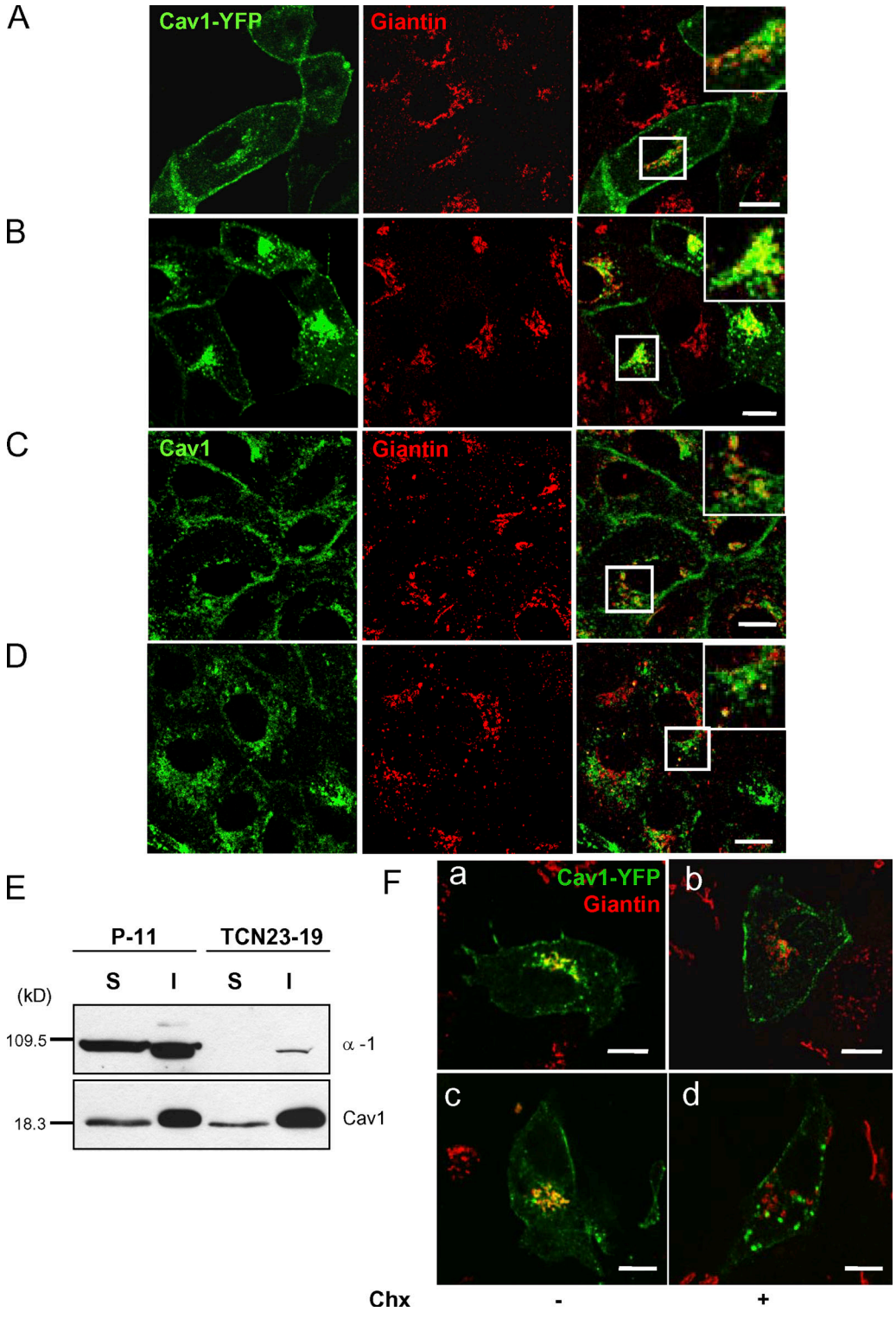

Figure 7. **Analyses of the Golgi pool of Cav1.** (A) P-11 and (B) TCN23-19 cells were transfected with Cav1-YFP. After 24 h, cells were fixed and stained for giantin and imaged. (C) P-11 and (D) TCN23-19 cells were immunostained for endogenous Cav1 and giantin. The white square area was enlarged and showed at the top right corner of the merged image to display the colocalization of giantin with Cav1. (E) P-11 and TCN23-19 cells were extracted by cold 0.1% Triton X-100 for 2 min as described in Materials and methods. Both soluble and insoluble fractions were collected and subjected to Western blot detection of α1 and Cav1. A representative blot of three independent experiments is shown. (F) P-11(a and b) and TCN23-19 (c and d) cells were transfected with Cav1-YFP for 3 h, then cells were fixed and stained for giantin (a and c). In b and d, transfected cells were treated with 10 μg/ml cycloheximide (Chx) for 3 h, then stained for giantin. Similar experiments were repeated at least four times. Images were taken by confocal microscope. Bars stand for 5 μm in all images.

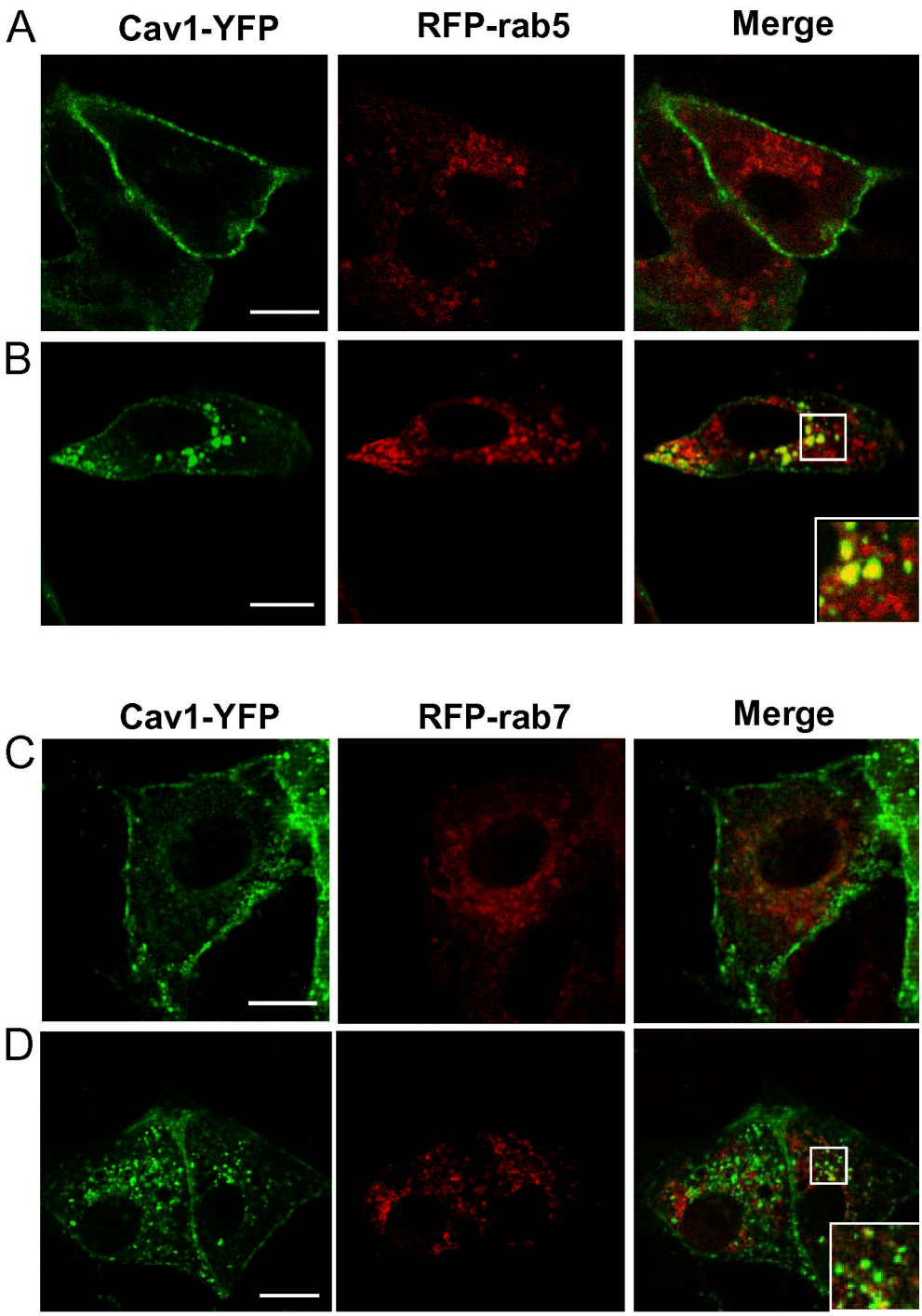

Figure 8. **Colocalization of Cav1-YFP with RFP-rab5, but not RFP-rab7, in Na/K-ATPase knockdown cells.** Both control P-11 (A and C) and knockdown TCN23-19 (B and D) cells were cotransfected with Cav1-YFP and RFP-rab5 or RFP-rab7 as indicated. Images were taken after 24 h of transfection. A clear colocalization of Cav1 with Rab5, but not Rab7, was seen in knockdown cells. Bar, 10 μm.

As depicted in Fig. 7 E, we found that a majority of the Cav1 was insoluble in cold 0.1% Triton X-100 in both control and knockdown cells, and that Na/K-ATPase knockdown did not change the amount of soluble Cav1.

It has been reported that the Golgi pool of Cav1 is dependent on new protein synthesis, but not on the exchange with Cav1 in the plasma membrane or in endosomes, because blocking new protein synthesis by cycloheximide was sufficient to empty endogenous Cav1 from the Golgi complex (Nichols, 2002). To further test whether the knockdown of Na/K-ATPase affects the Golgi exit of Cav1, we transfected both control and knockdown cells with Cav1-YFP for 3 h. As depicted in Fig. 7 F, before addition of cycloheximide, both cells contained a Golgi pool of Cav1 as indicated by the giantin colocalization (Fig. 7 F, a and c). After protein synthesis was blocked by cycloheximide, both P-11 and TCN23-19 cells were able to empty this pool of

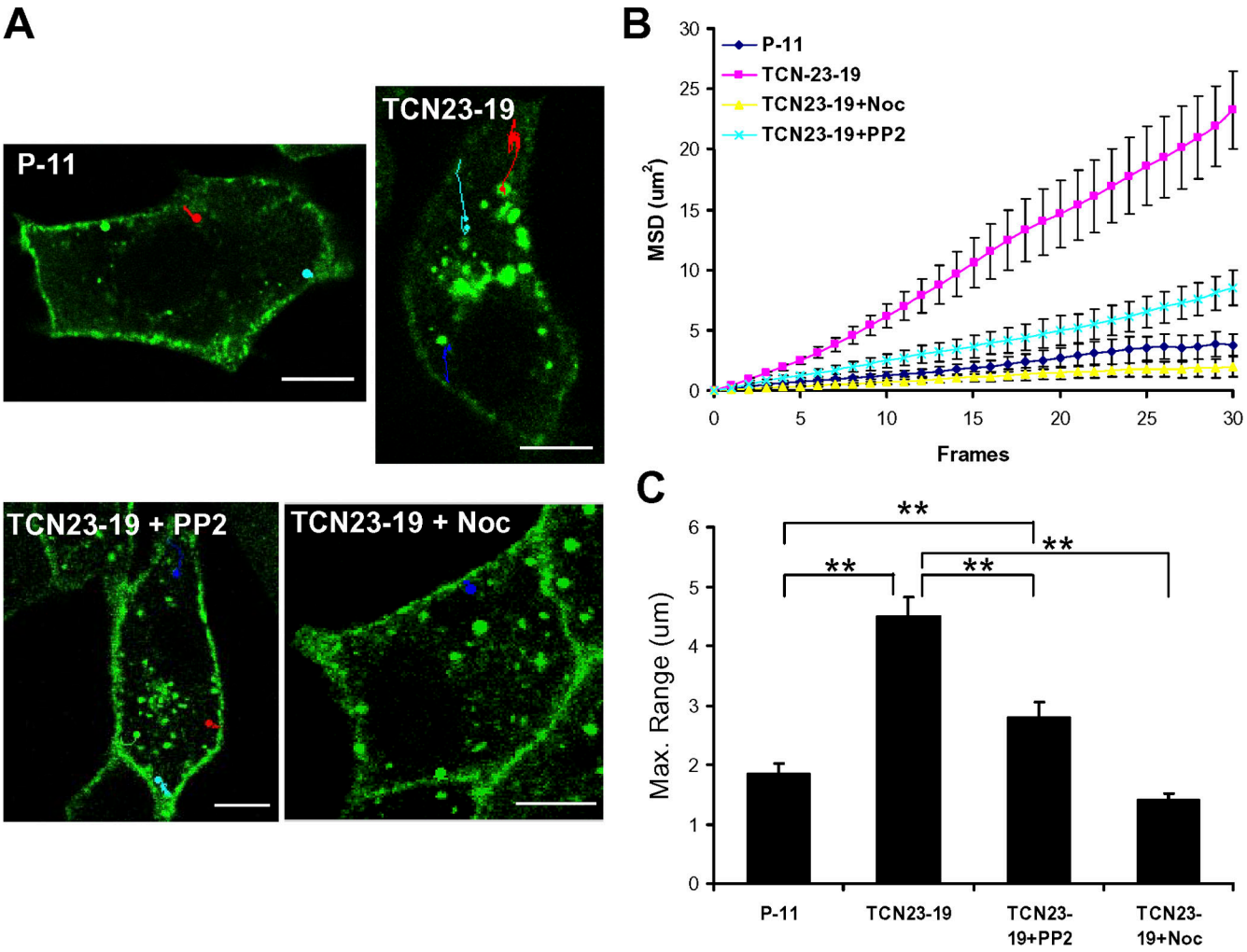

Figure 9. **Effects of Na/K-ATPase knockdown on the mobility of Cav1-YFP–positive vesicles.** Control (P-11) and knockdown (TCN23-19) cells were transfected with Cav1-YFP, and Cav1-YFP–positive vesicles moving underneath or away from the plasma membrane were monitored using time-lapse confocal microscopy. (A) Trajectories of the moving Cav1-YFP–positive vesicles in control, knockdown cells, as well as in the knockdown cells that were treated with 5 μM of nocodazole (Noc) or 2 μM of PP2. The moving path of each moving vesicle was shown as a line and ended with a dot. The images are the overlay of the trajectory with the synergized snapshots from Videos 1, 3, 5, and 7. (B) The mean square distance (MSD) each Cav1-YFP–positive vesicle traveled between each frame was measured, and the mean ± SE from at least 30 measurements is shown in the graph. (C) The average of maximal range of each vesicle traveled was calculated and shown in the bar graph. Values are mean ± SE of 16 separate experiments of each cell line. **, $P < 0.01$ between groups as indicated. Bar, 10 μm.

Cav1-YFP (Fig. 7 F, b and d). As expected, in the knockdown cells we observed more Cav1-YFP–positive vesicles in the cytoplasm than that in the control cells. Together, the data indicate that Cav1 can exit from the Golgi complex in the knockdown cells. Therefore, knockdown of the Na/K-ATPase is likely to affect either endocytosis or exocytosis (or both) of Cav1, resulting in a net accumulation of Cav1-positive vesicles.

Cav1-YFP–positive vesicles in the knockdown cells are colocalized with rab5, but not rab7

The fractionation data in Fig. 1 indicated that knockdown of Na/K-ATPase caused a higher density migration of intracellular Cav1. Because prior studies demonstrated that Cav1 vesicles could fuse into endosomes during endocytosis (Pelkmans et al., 2001), we reasoned that this type of fusion might take place in the Na/K-ATPase knockdown cells, resulting in increases in floating density and the accumulation of large size Cav1-positive vesicles. To test this hypothesis, cells were cotransfected with Cav1-YFP and RFP-rab5 or RFP-rab7. Confocal images showed that many large Cav1-YFP–positive vesicles were indeed colocalized with RFP-rab5 in TCN23-19, but not in P-11 cells (Fig. 8, A and B). These results indicated that knockdown of Na/K-ATPase is likely to stimulate the endocytosis of Cav1. Interestingly, no colocalization was detected between Cav1-YFP and RFP-rab7, a late endosome marker (Fig. 8, C and D).

The Na/K-ATPase knockdown increases the endocytosis of Cav1

The above data indicated that knockdown of Na/K-ATPase increased an internal accumulation of Cav1 vesicles. To test whether this is a result of increased endocytosis, we monitored Cav1-YFP–positive vesicle movement in both control and TCN23-19 cells. As depicted in Fig. 9 A, we could observe some endocytic

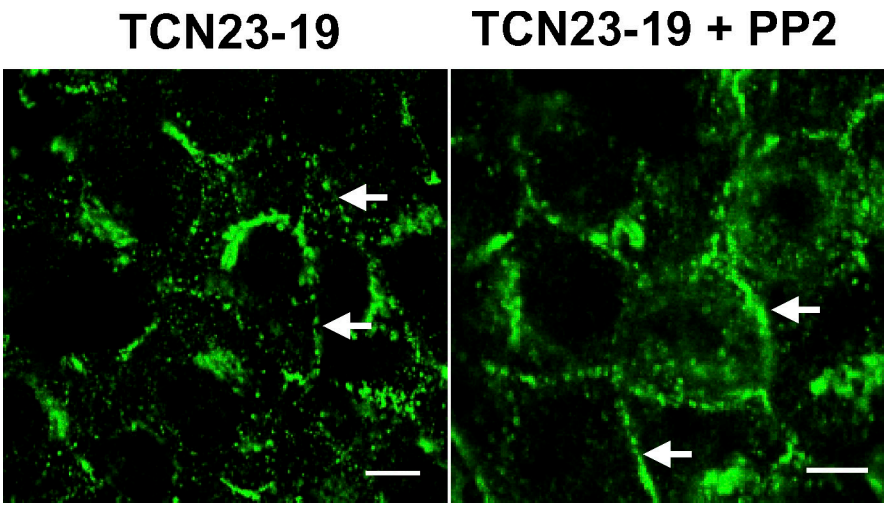

Figure 10. **Effect of Src inhibitor PP2 on the cellular distribution of Cav1.** TCN23-19 cells were treated with 2 μM of PP2 for 5 h; afterward, both control and PP2-treated cells were stained for Cav1. The plasma membrane signals were labeled by solid arrows in both treated and untreated cells to illustrate the recovery of Cav1 signal in the plasma membrane of PP2-treated cells. A set of representative images from three experiments is shown. Bar, 5 μm.

events and occasionally a long-range directional movement of the internalized Cav1 vesicles toward the perinuclear area in the control P-11 cells (also see Videos 1 and 2, available at http://www.jcb.org/cgi/content/full/jcb.200712022/DC1). This is consistent with what has been reported in other cells (Pelkmans and Zerial, 2005). Two important differences were noticed immediately when the same experiment was conducted in TCN23-19 cells. First, we observed that more Cav1-YFP–positive vesicles pinched off from the plasma membrane. Second, many of the internalized vesicles underwent a long-range (over distances of 2 μm) and directional movement toward the perinuclear area (Fig. 9 A and Videos 3 and 4, available at http://www.jcb.org/cgi/content/full/jcb.200712022/DC1). Quantitatively, there was a 2.6 ± 0.4-fold ($n = 40$) increase in the number of fission events in TCN23-19 cells. To describe the trajectory of moving Cav1-YFP–positive vesicles, we adopted the computational methods described by others (Qian et al., 1991; Saxton and Jacobson, 1997; Jin and Verkman, 2007) and analyzed mean square displacement (MSD), i.e., the average of the square of the distance moved by the vesicle between image frames. As shown in Fig. 9 B, the MSD versus time plot for the trajectory of moving Cav1-YFP–positive vesicles in control P-11 cells resembled that of confined diffusion (Haggie et al., 2006; Nudelman and Louzoun, 2006), consistent with what was reported previously (Pelkmans and Zerial, 2005). In contrast, the MSD plot became linear in the Na/K-ATPase knockdown cells, which is similar to the MSD plot for simple diffusion. When the moving distance was calculated, the maximum range that vesicles traveled in TCN23-19 cells was 4.51 ± 0.32 μm, much longer than the 1.86 ± 0.17 μm detected in control cells (Fig. 9 C).

To further confirm that knockdown of the Na/K-ATPase increases the mobility of Cav1, we determined fluorescence recovery after photobleaching (FRAP). Cells were transiently transfected with Cav1-YFP for 24 h, and a periphery segment of a transfected cell was bleached. Afterward, the movement of Cav1 into the bleached area over the distance of 2 μm was monitored as a function of time using confocal microscopy. Consistent with previous reports in other types of cells (Kasahara et al., 2004; Tagawa et al., 2005), some Cav1-YFP were able to move into the bleaching area, but the percentage of recovery was quite low in control P-11 cells. On the other hand, an increase in recovery was observed in TCN23-19 cells. When total fluorescence was measured in both control and the knockdown cells over 15 min, we detected a 9.0 ± 1.5% of recovery in the control P-11 cells and a 16 ± 1.0% recovery in TCN23-19 cells ($n = 6$, $P < 0.01$).

Involvement of Src

It is known that Src plays an important role in controlling Cav1 endocytosis (Sharma et al., 2004; Pelkmans and Zerial, 2005; Le Lay et al., 2006). We have reported that there is a pool of Na/K-ATPase–interacting Src in LLC-PK1 cells (Liang et al., 2006; Tian et al., 2006). Binding of Src to this pool of Na/K-ATPase keeps Src in an inactive state and knockdown of Na/K-ATPase releases this pool of Src, resulting in an increase in basal Src activity. Thus, the Na/K-ATPase knockdown-induced Src activation could be responsible for the observed increase in the mobility of Cav1 vesicles in TCN23-19 cells. To test this postulation, TCN23-19 cells were treated with PP2, a Src family kinase inhibitor, for 5 h and then immunostained for Cav1. Cell imaging showed that PP2 treatment caused a significant increase in plasma membrane Cav1 signal (42.6 ± 1.5% v. 26 ± 1%; $n = 28$; $P < 0.01$) (Fig. 10). The above experiment was repeated in Cav1-YFP transfected cells, and showed similar result (44.2 ± 2% in PP2 treated cells vs. 32 ± 1% in nontreated TCN23-19 cells; $n = 30$; $P < 0.01$). In accordance, we found that PP2 significantly reduced the mobility of Cav1-YFP–positive vesicles in TCN23-19 cells (Fig. 9, B and C and Videos 5 and 6, available at http://www.jcb.org/cgi/content/full/jcb.200712022/DC1).

The Na/K-ATPase knockdown-induced movement of Cav1 is microtubule dependent

It has been reported by several groups that disruption of microtubule (MT) abolished trafficking of Cav1 vesicles (Mundy et al., 2002; Tagawa et al., 2005; Head et al., 2006). Thus, we tested whether the increased movement of Cav1 vesicle in the Na/K-ATPase knockdown cells is MT dependent. As depicted in Fig. 9 and Videos 7 and 8 (available at http://www.jcb.org/cgi/content/full/jcb.200712022/DC1), addition of nocodazole

abolished the effects of the knockdown of Na/K-ATPase on the movement of Cav1-positive vesicles. Interestingly, the still image from the video of TCN23-19 + nocodazole showed that the plasma membrane localization of Cav1-YFP seemed to be recovered when compared with that in the untreated TCN23-19 cells (Fig. 9 A). However, there were still a few large Cav1-YFP–positive vesicles residing in the cytoplasm (Fig. 9 A). This should not be a surprise because these large vesicles in the cytoplasm are probably the remnants of the accumulated vesicles before nocodazole treatment.

Discussion

We have demonstrated here that the Na/K-ATPase interacts with Cav1, and regulates the Cav1 membrane trafficking and ultimately the formation of caveolae in cultured cells. Moreover, we have uncovered the importance of the α1 CBM in the interaction between Na/K-ATPase and Cav1. Finally, the pool of Na/K-ATPase–interacting Src appears to play an important role in this newly identified regulation. All together, our new findings unravel a novel function of the Na/K-ATPase and provide new insights into the molecular mechanism of membrane trafficking of Cav1.

The Na/K-ATPase interacts with Cav1

In this paper, we showed that knockdown of Na/K-ATPase reduced the amount of α1 detected in fraction 4/5 and subsequently redistributed Cav1 from this fraction to high density fractions. This was further confirmed by imaging analyses showing decreases in the plasma membrane pool of Cav1 with a concomitant accumulation of cytosolic Cav1 vesicles. Consistently, electron microscopy data demonstrated a reduction of surface caveolae in the knockdown cells. In addition, colocalization analyses indicated that some of the internalized Cav1 might reside in early endosomes.

Cav1 is an integral membrane protein with both N and C termini located intracellularly. Studies have identified the scaffolding domain (amino acid residue 81–101) as being important for targeting and concentrating Cav1 to caveolae (Schlegel and Lisanti, 2000). It is known that this scaffolding domain interacts with the CBM present in many membrane and soluble proteins (Couet et al., 1997; Liu et al., 2002). In addition, it is also important for the interaction between Cav1 and cholesterol (Murata et al., 1995; Fielding et al., 2002). We previously showed that the Na/K-ATPase was highly concentrated in the caveolin-enriched fractions in LLC-PK1 cells and that both proteins existed in the same signalosome and could be coimmunoprecipitated by either anti-Cav1 or anti-α1 antibodies. In vitro binding assays also demonstrated that the Na/K-ATPase directly interacted with the Cav1 N terminus (Wang et al., 2004). Consistent with these findings, we showed here that CFP-Cav1 and YFP-α1 resided close enough to yield a strong FRET signal in the plasma membrane. Structurally, the α1 subunit of Na/K-ATPase contains two potential CBM, one at the N terminus and the other at the C terminus. Phylogenic analysis shows that the N-terminal CBM is highly conserved and appears to be acquired during evolution before the C-terminal CBM (Xie and Cai, 2003). Interestingly, mutation of the N-terminal CBM abolished the FRET between the YFP-α1 and CFP-Cav1. Moreover, expression of mCBM α1 failed to rescue the defect in cellular Cav1 distribution. These findings, together with our prior in vitro binding data (Wang et al., 2004), suggest that the N-terminal CBM of α1 subunit is involved in the interaction with Cav1. This postulation is consistent with the newly released 3D structure of Na/K-ATPase (Morth et al. 2007), which clearly shows that the CBM at the N terminus of α1 is in close proximity to the cytosolic plasma membrane surface and highly exposed, whereas the other CBM at the C terminus of α1 is buried in the transmembrane area and exposed to the extracellular surface. However, it is important to point out that domains other than the N-terminal CBM may also participate or contribute to this interaction because Cav1 does not simply interact with CBM-containing proteins (Parton and Simons, 2007). Resolution of this structural issue requires further investigation.

It has been proposed that the interaction between Cav1 and the membrane receptors is important for targeting these receptors to caveolae. However, unlike many other receptors and ion channels, the Na/K-ATPase is a highly abundant membrane protein in many types of cells (Baker and Willis, 1969, 1970; McCall, 1979). For example, the number of Na/K-ATPase in the plasma membrane of LLC-PK1 cells is ∼1 million per cell with half residing in caveolae (Liang et al., 2007). Thus, it is unlikely that the caveolae residence of such a large number of Na/K-ATPase is due to a Cav1-mediated "trapping". On the contrary, we believe that the Na/K-ATPase may serve as a scaffold and play a role in stabilizing the plasma membrane distribution of Cav1 via this interaction. Nevertheless, several uncertainties should be noted. First, the interpretation of our new findings, at least at the present stage, should be limited to cells we have tested. Second, although we did not observe an overt defect in the Golgi exit of the newly synthesized Cav1, we could not rule out that there may be a slowdown in the knockdown cells because our approach was not intended to measure the speed of protein exit from the Golgi complex. On the other hand, it is important to note that knockdown of Na/K-ATPase apparently did not affect the oligomerization of Cav1 and its interaction with lipid rafts because there was no difference in detergent solubility of Cav1 between P-11 and TCN23-19 cells. This is important because several proteins have been identified to affect Cav1 distribution through altering Cav1 Golgi exit (Jones et al., 2004; Cubells et al., 2007). Finally, although we observed that some Cav1 resided in early endosomes in the knockdown cells, it remains to be tested whether this residence accounts for the observed shifts of Cav1 from light to heavy density fractions (Fig. 1).

The Na/K-ATPase regulates Cav1 trafficking

FRAP analysis has indicated that the majority of plasma membrane Cav1 is highly immobile in many cell types (Pelkmans et al., 2001; Thomsen et al., 2002). This is certainly true in LLC-PK1 cells. However, the plasma membrane Cav1 can be mobilized by many factors including changes in cellular amount of Cavin and cholesterol, as well as activation of protein kinases. For instance, addition of SV40 to cells stimulates Cav1

endocytosis and increased the formation of large size Cav1-positive early endosomes, which appears to require Src activation. Similarly, we found that knockdown of the Na/K-ATPase stimulated the endocytosis of Cav1 and increased the long-range movement of Cav1-positive vesicles (Fig. 9). Interestingly, in comparison to Cavin (Hill et al., 2008), knockdown of the Na/K-ATPase not only reduced the surface number of caveolae, but also concomitantly increased Cav1-positive vesicles in the cytoplasm. Mechanistically, we have demonstrated that the Na/K-ATPase interacts and keeps Src in an inactive state (Tian et al., 2006). Thus, we believe that the Na/K-ATPase depletion-induced Src activation may be responsible for the observed increases in the movement of Cav1. This postulation is supported by the data presented in Figs. 9 and 10. Moreover, we have recently observed that knockdown of Na/K-ATPase also decreased the plasma membrane and ultimately the ER cholesterol, resulting in the activation of sterol regulatory element-binding protein 2 (SREBP2) and increased expression of HMG-CoA reductase (unpublished data). Thus, reduction of the plasma membrane cholesterol may work in concert with Src activation in regulation of Cav1 endocytosis.

As shown in Fig. 9, knockdown of the Na/K-ATPase stimulated the long-range directional movement of Cav1-positive vesicles toward the perinuclear region. Such movement has been well characterized and can be stimulated when the cells are exposed to stimuli such as SV40 (Pelkmans et al., 2001; Pelkmans and Zerial, 2005). Mechanistically, such movements are known to be mediated by the changes in the cortical actin cytoskeleton, and the activation of microtubule-dependent trafficking (Mundy et al., 2002; Pelkmans et al., 2002; Pelkmans and Zerial, 2005; Tagawa et al., 2005). Consistently, we found that disruption of microtubules by nocodazole abolished the effects of Na/K-ATPase knockdown on Cav1 trafficking.

Because the Na/K-ATPase interacts directly with ankyrin (Devarajan et al., 1994; Jordan et al., 1995), it is possible that depletion of Na/K-ATPase could also affect cellular actin cytoskeleton structure, which may contribute to the increased mobility of Cav1. When we visualized the overall distribution of actin microfilaments using immunofluorescence and laser scanner confocal microscopy, we failed to detect significant differences between the control and Na/K-ATPase knockdown cells (unpublished data). However, we cannot rule out the local and transient change of actin cytoskeleton during the short- and long-range movement of Cav1 vesicles, as what happened in SV40-triggered internalization of Cav1 (Pelkmans et al., 2002).

In short, our new findings demonstrated that the Na/K-ATPase interacted with Cav1 and regulated the trafficking of Cav1. To this end, it is important to mention that Na/K-ATPase also interacts with many proteins including arrestins and spinophilin that are involved in control of formation and trafficking of clathrin-coated vesicles (Kimura et al., 2007). Functionally, the Na/K-ATPase internalizes in a clathrin-dependent manner after the cells are stimulated by hormones such as dopamine and ouabain (Chibalin et al., 1997; Liu et al., 2004). Interaction with arrestins facilitates the endocytosis. On the other hand, binding of spinophilin to the Na/K-ATPase inhibits the association of arrestins to the enzyme, and thus slows the endocytosis. In view of our new findings, it will be of interest to test whether the Na/K-ATPase plays a role in regulation of clathrin-dependent cellular trafficking. Interestingly, the early studies demonstrated that the Na/K-ATPase appeared to be important for endosomal pH regulation (Cain et al., 1989; Fuchs et al., 1989).

Cav1 and Na/K-ATPase–mediated signal transduction

Many membrane receptors, protein kinases, and other signaling proteins reside in caveolae and can be coimmunoprecipitated by anti-Cav1 antibodies. Moreover, the Cav1 scaffolding domain has been shown to inhibit the function of many signaling molecules (Williams and Lisanti, 2004). These findings have led to the hypothesis that caveolae functions as a universal signaling regulator. Indeed, we and others have demonstrated that the Na/K-ATPase resides in caveolae and that caveolar Na/K-ATPase interacts with Src to form a functional receptor complex. Binding of both endogenous and exogenous cardiotonic steroids such as ouabain to this receptor complex activates the Na/K-ATPase–associated Src, resulting in increases in protein tyrosine phosphorylation and the generation of second messengers (Wang et al., 2004; Yuan et al., 2005; Liang et al., 2006; Tian et al., 2006). Moreover, depletion of either Cav1 or cholesterol redistributes Na/K-ATPase and abolishes ouabain-induced signal transduction. It also prevents the agonist-induced endocytosis of the Na/K-ATPase signaling complexes (Liu et al., 2005). Thus, the direct interaction between the Na/K-ATPase and Cav1 not only regulates Cav1 trafficking, but also plays an essential role in the formation of a functional Na/K-ATPase signaling complex. Needless to say, the validity of this hypothesis has to be further confirmed in caveolin knockout mice as the role of Cav1 in many signaling events has been questioned by recent in vivo studies (Souto et al., 2003; Gonzalez et al., 2004). Nevertheless, we believe that this newly identified functional interaction between the Na/K-ATPase and Cav1 serves as an excellent model for further exploring the biological role of Cav1 and caveolae in signal transduction and animal physiology.

Materials and methods

Materials and reagents

The antibodies used and their sources are as follows: the anti-Cav1 polyclonal antibody, anti-EEA-1, anti-GM130, goat anti–rabbit secondary antibody, and goat anti–mouse secondary antibody were obtained from Santa Cruz Biotechnology, Inc. Other anti-Cav1 monoclonal and polyclonal antibodies and anti-calnexin antibody were from BD Biosciences. The monoclonal anti-α1 antibody and polyclonal anti-α1 antibody were obtained from Millipore. EM-grade gold conjugates, goat anti–rabbit IgG (10-nm gold), were obtained from British Biocell International. All secondary antibodies used in Western blot were conjugated to horseradish peroxidase. Therefore, the immunoreactive bands were developed using the chemiluminescence kit (Thermo Fisher Scientific).

Plasmid constructs, cell culture, and transfection

To construct the fluorescent protein fused target protein, rat Na/K-ATPase α1 subunit cDNA was inserted in-frame into pEYFP-C1. Human Cav1 cDNA was PCR cloned and inserted in-frame into pECFP-C1/N1 vectors. Rat α1 pump-null mutant (D371N) and CBM mutant (Phe^{92}-XXXX-Phe^{97}-XX-Phe^{100} to Phe^{92}-XXXX-Ala^{97}-XX-Ala^{100}, F97A/F100A) were created by PCR-based site-directed mutagenesis with the QuikChange site-directed mutagenesis kit from Stratagene. RFP-rab5 and RFP-rab7 were requested from www.addgene.org. All constructs were verified by DNA sequencing.

The knockdown cell lines (A4-11, PY-17, and TCN23-19), and the control P-11 cell line were derived from pig LLC-PK1 cells as previously reported (Liang et al., 2006). The cells were cultured in DMEM containing 10% fetal bovine serum, penicillin (100 units/ml), streptomycin (100 µg/ml), and 1 µg/ml puromycin. When cell cultures reached ~90% confluence, cells were used for the experiments. Cells were transfected with various plasmids or empty vectors using Lipofectamine 2000 as described previously (Wang et al., 2004; Tian et al., 2006). Experiments were performed 24 h after transfection unless indicated otherwise.

Purification of caveolin-rich membrane fractions, Triton X-100 extraction, and Western blot

Caveolin-rich membrane fractions were obtained by means of sucrose gradient fractionation (Liu et al., 2003; Wang et al., 2004). In brief, LLC-PK1 cells were collected with 500 mM sodium carbonate, pH 11.0, and then homogenized. The homogenate was then adjusted to 45% sucrose by addition of 2 ml of 90% sucrose prepared in MBS (25 mM Mes and 0.15 M NaCl, pH 6.5) and placed at the bottom of an ultracentrifuge tube. The ultracentrifuge tubes were then loaded with 4 ml of 35% sucrose and 4 ml of 5% sucrose (both in MBS containing 250 mM sodium carbonate) and centrifuged at 39,000 rpm for 16–20 h in an SW41 rotor (Beckman Coulter). A light-scattering band at the interface between the 5 and 35% sucrose gradients was observed. 11 gradient fractions of 1 ml were collected from the top to the bottom of the centrifuge tube. Equal volumes of each fraction were analyzed by Western blot.

Extraction of cold Triton X-100 soluble protein was done as described previously (Pol et al., 2005). In brief, LLC-PK1 cells were washed twice with cold PBS. Then they were extracted for 2 min by immersion into 250 µl of ice-cold 0.1% Triton X-100 solution containing 10 mM Tris, pH 7.5, 150 mM NaCl, 5 mM EDTA, and protease and phosphatase inhibitors. Nuclei and unbroken cells were removed from the soluble supernatant by centrifugation at 2,000 rpm for 5 min at 4°C in an Eppendorf tube. The pellet was dissolved in 250 µl RIPA buffer. Equal volumes of the soluble and insoluble fractions were subjected to Western blot analysis.

Immunofluorescence and imaging analysis

Imaging study was performed as described previously (Tian et al., 2006). Cells were cultured for 24 h on glass coverslips. After being fixed with 4% paraformaldehyde, the cells were permeabilized for 20 min with 0.1% saponin in PBS. The cells were washed again with PBS and blocked with Signal Enhancer (Invitrogen). Primary antibodies were diluted in 3% BSA in PBS and coverslips were incubated with antibodies overnight at 4°C (Pol et al., 2005). After three washes with PBS, AlexaFluor 546/488–conjugated antibodies were added and incubated for 1 h at room temperature. Samples were washed and mounted onto slides. Cells were visualized using an inverted confocal laser scanning microscope (DM IRE2; Leica) equipped with a 63x/1.3 oil objective. An argon and a helium/neon laser were used for double fluorescence with excitation at 433 nm, 515 nm and emission at 505–510 nm, and 566–620 nm, respectively (Tian et al., 2006). To avoid the cross-talk between the two fluorescent dyes, we used the sequential method featured by the Leica confocal microscope to acquire the images for measuring colocalization of the two proteins. To quantify the localization changes of Cav1 in control and knockdown cells, Cav1 fluorescence within 1 µm of the cell surface is considered PM and its proximity; fluorescence internal and away from this zone is considered intracellular region. Fluorescence intensity of total cell area (Ft) and the intracellular region (Fi) were measured by ImageJ, the percentage of Cav1 localized on the PM was calculated by (Ft − Fi)/Ft. Values are mean ± SE from 30–50 cells in at least 10 independent experiments.

Electron microscopy

Cell samples were prepared as described previously (Wu et al., 1997; Cubells et al., 2007). In brief, cell monolayers on 10-cm dishes were rinsed with PBS and fixed with 3% paraformaldehyde and 0.5% glutaraldehyde in 0.2 M sodium cacodylate (pH 7.4) for 1 h at room temperature. Cells were gently scraped from the dishes with a rubber policeman, collected, and pelleted. After three 30-min rinses each in the cacodylate buffer, pellets were post-fixed in 1% OsO_4 (s-collidine buffered) for 90 min. Finally, samples were embedded in Spurr low viscosity embedding media (Electron Microscopy Sciences). Ultrathin sections were analyzed with an electron microscope (CM-10; Philips). The number of surface caveolae (noncoated 30–80-nm surface flask-shaped membrane invaginations) was determined in random fields of sections from images acquired at the same magnification (34,000). More than 40 cells were examined for each cell line.

To perform immunogold staining (Wu et al., 1997), cells cultured in 35-mm tissue culture wells were fixed with 3% paraformaldehyde and 0.5% glutaraldehyde for 1 h, washed with 0.2 M Hepes (pH 7.3), and cell pellets were collected. After quenching with 0.5 M NH_4Cl for 1 h, cell pellets were washed with fresh sodium cacodylate buffer and dehydrated in a graded series of ethanols. Then cells were embedded in LR-white resin, and polymerized at 55°C for 2 d and sectioned using a Leica ultramicrotome. The sections were first blocked with 1% fish gelatin in 0.1 M Hepes for 30 min, and then probed with rabbit anti-caveolin antibody (1:10 dilution) for 2 d. Grids were washed three times with 0.2 M NaCl, and subsequently incubated with 10-nm gold conjugated goat anti–rabbit IgG (1:100 dilution) for 1 h. Afterward, grids were washed three times with high salt solution (2.5 M NaCl), post-stained with aqueous uranyl acetate for 25 min, and washed five times with distilled H_2O. Gold particles were analyzed using an electron microscope (CM-10; Philips). Images were randomly taken from sections prepared from three separate experiments. Quantification of the distribution of gold particles was done as described previously (Hill et al., 2008).

FRET analysis by acceptor photobleaching

As previously described (Tian et al., 2006), CFP-Cav1 and YFP-rat α_1, D371N mutant, or CBM mutant were cotransfected into TCN23-19 cells. After 24 h of culture, cells on glass coverslips were fixed with 4% paraformaldehyde for 30 min at room temperature and washed twice with PBS solution. The coverslips were then mounted and used for FRET measurement with the Leica confocal microscope (DM IRE2; Leica). The YFP-tagged protein was photobleached by applying full power of 515-nm laser, and the emission of CFP excited by 456-nm laser was recorded before (D_{pre}) and after (D_{post}) YFP photobleaching. The FRET efficiency was then calculated by the Ep value, corrected ratio of $(D_{post} - D_{pre})/D_{pre}$ in the photobleached region comparing it to the nonbleached region in the same experiment.

FRAP analysis

We followed the protocol as described previously (Kasahara et al., 2004; Tagawa et al., 2005). In brief, Cav1-YFP was transfected into control and knockdown cells for 24 h, and then the cells were loaded into an Attofluor cell chamber (Invitrogen) in physiological salt solution containing 100 mM NaCl, 5 mM KCl, 20 mM Hepes, 25 mM $NaHCO_3$, 1 mM $CaCl_2$, 1.2 mM $MgCl_2$, 1 mM NaH_2PO_4, and 10 mM D-glucose. The chamber was mounted onto a confocal microscope (DM IRE2; Leica) at room temperature. FRAP analysis was performed by using Leica confocal software. A picture was taken at prebleach, and then the selected area was under full-power bleaching for 20 times. Recovery was monitored by scanning for 60 min at 20-s intervals at low laser power (15% power). Images were processed using ImageJ. Relative fluorescence of recovery = $[(\text{b-FI}_{[15]}/\text{t-FI}_{[15]}) - (\text{b-FI}_{[0]}/\text{t-FI}_{[0]})]/\text{b-FI\_pre/t-FI\_pre}$, where $\text{b-FI}_{[0]}$ is the intensity of the bleached area at time 0 s after bleaching, $\text{t-FI}_{[0]}$ is the total intensity of the cell at time 0 s after bleaching, $\text{b-FI}_{[15]}$ is the intensity of bleached area after 15 min of recovery, and $\text{t-FI}_{[15]}$ is the total intensity of the cell after 15 min of recovery. b-FI_pre and t-FI_pre is the intensity of bleached area and total cell before photobleaching.

Live particle tracking

Cells transfected with Cav1-YFP were monitored by confocal microscope (DM IRE2; Leica) using time-lapse imaging under 12% power of laser light at 488 nm for 30 min. The trajectory of the moving Cav1-YFP–positive vesicles were generated by comparing each frame and measured by Manual Tracking using ImageJ. The resolution limit to the confocal laser microscope is ~0.5 µm. Thus, only Cav1-YFP–positive vesicles with a diameter more than 1 µm and moving away from the plasma membrane were studied. Mean square displacement (MSD) was calculated where the $x(t)$ and $y(t)$ are particle positions at time t, N is the total number of frames, n is the number of time intervals, and j is a positive integer (Qian et al., 1991; Jin et al., 2007).

$$MSD(n\Delta t) = \sum_{j=0}^{N-1-n} \{[x(j\Delta t + n\Delta t) - x(j\Delta t)]^2 + [y(j\Delta t + n\Delta t) - y(j\Delta t)]^2\} / (N - 1 - n).$$

The range of particle diffusion was calculated as

$$Range(n\Delta t) = \{[x(j\Delta t + n\Delta t) - x(j\Delta t)]^2 + [y(j\Delta t + n\Delta t) - y(j\Delta t)]^2\}^{1/2}.$$

The maximal range was acquired by calculation of the absolute distance between each position on the trajectory respective to the starting position

(Pelkmans et al., 2002). The averaged maximum distance of 18–29 trajectories from each cell line was taken and presented as mean ± SE.

Data analysis

Data are given as mean ± SE. Statistical analysis was performed using Student's *t* test and significance was accepted at $P < 0.05$.

Online supplemental material

Videos (1–8) for Fig. 9 show trajectories of moving Cav1-YFP–positive vesicles in indicated cells. Fig. S1 shows that the expression of α1 rescues Cav1 distribution in PY-17 cells. Online supplemental material is available at http://www.jcb.org/cgi/content/full/jcb.200712022/DC1.

We are grateful for skilled technical support from Manoranjani Tillerkeratne and Michele Lewandowski. We also appreciate Martha Heck for editing the manuscript.

This work was supported by National Institutes of Health Grants HL-36573, HL-67963, and GM-78565. L.E.M. Quintas was the recipient of a postdoctoral fellowship from CNPq, Brazil.

Submitted: 6 December 2007
Accepted: 20 August 2008

References

Aizman, O., P. Uhlen, M. Lal, H. Brismar, and A. Aperia. 2001. Ouabain, a steroid hormone that signals with slow calcium oscillations. *Proc. Natl. Acad. Sci. USA.* 98:13420–13424.

Anderson, R.G. 1998. The caveolae membrane system. *Annu. Rev. Biochem.* 67:199–225.

Baker, P.F., and J.S. Willis. 1969. On the number of sodium pumping sites in cell membranes. *Biochim. Biophys. Acta.* 183:646–649.

Baker, P.F., and J.S. Willis. 1970. Potassium ions and the binding of cardiac glycosides to mammalian cells. *Nature.* 226:521–523.

Balasubramanian, N., D.W. Scott, J.D. Castle, J.E. Casanova, and M.A. Schwartz. 2007. Arf6 and microtubules in adhesion-dependent trafficking of lipid rafts. *Nat. Cell Biol.* 9:1381–1391.

Brazer, S.C., B.B. Singh, X. Liu, W. Swaim, and I.S. Ambudkar. 2003. Caveolin-1 contributes to assembly of store-operated Ca2+ influx channels by regulating plasma membrane localization of TRPC1. *J. Biol. Chem.* 278:27208–27215.

Cain, C.C., D.M. Sipe, and R.F. Murphy. 1989. Regulation of endocytic pH by the Na+,K+-ATPase in living cells. *Proc. Natl. Acad. Sci. USA.* 86:544–548.

Chen, Y., T. Cai, C. Yang, D.A. Turner, D.R. Giovannucci, and Z. Xie. 2007. Regulation of inositol 1,4,5-trisphosphate receptor-mediated calcium release by the Na/K-ATPase in cultured renal epithelial cells. *J. Biol. Chem.* 283:1128–1136.

Chibalin, A.V., A.I. Katz, P.O. Berggren, and A.M. Bertorello. 1997. Receptor-mediated inhibition of renal Na(+)-K(+)-ATPase is associated with endocytosis of its alpha- and beta-subunits. *Am. J. Physiol.* 273:C1458–C1465.

Couet, J., M. Sargiacomo, and M.P. Lisanti. 1997. Interaction of a receptor tyrosine kinase, EGF-R, with caveolins. Caveolin binding negatively regulates tyrosine and serine/threonine kinase activities. *J. Biol. Chem.* 272:30429–30438.

Cubells, L., S. Vila de Muga, F. Tebar, P. Wood, R. Evans, M. Ingelmo-Torres, M. Calvo, K. Gaus, A. Pol, T. Grewal, and C. Enrich. 2007. Annexin A6-induced alterations in cholesterol transport and caveolin export from the Golgi complex. *Traffic.* 8:1568–1589.

Devarajan, P., D.A. Scaramuzzino, and J.S. Morrow. 1994. Ankyrin binds to two distinct cytoplasmic domains of Na,K-ATPase alpha subunit. *Proc. Natl. Acad. Sci. USA.* 91:2965–2969.

Edwards, A., and T.L. Pallone. 2007. Ouabain modulation of cellular calcium stores and signaling. *Am. J. Physiol. Renal Physiol.* 293:F1518–F1532.

Fielding, P.E., J.S. Russel, T.A. Spencer, H. Hakamata, K. Nagao, and C.J. Fielding. 2002. Sterol efflux to apolipoprotein A-I originates from caveolin-rich microdomains and potentiates PDGF-dependent protein kinase activity. *Biochemistry.* 41:4929–4937.

Fuchs, R., S. Schmid, and I. Mellman. 1989. A possible role for Na+,K+-ATPase in regulating ATP-dependent endosome acidification. *Proc. Natl. Acad. Sci. USA.* 86:539–543.

Glenney, J.R. Jr. 1989. Tyrosine phosphorylation of a 22-kDa protein is correlated with transformation by Rous sarcoma virus. *J. Biol. Chem.* 264:20163–20166.

Gonzalez, E., A. Nagiel, A.J. Lin, D.E. Golan, and T. Michel. 2004. Small interfering RNA-mediated down-regulation of caveolin-1 differentially modulates signaling pathways in endothelial cells. *J. Biol. Chem.* 279:40659–40669.

Haggie, P.M., J.K. Kim, G.L. Lukacs, and A.S. Verkman. 2006. Tracking of quantum dot-labeled CFTR shows near immobilization by C-terminal PDZ interactions. *Mol. Biol. Cell.* 17:4937–4945.

Head, B.P., H.H. Patel, D.M. Roth, F. Murray, J.S. Swaney, I.R. Niesman, M.G. Farquhar, and P.A. Insel. 2006. Microtubules and actin microfilaments regulate lipid raft/caveolae localization of adenylyl cyclase signaling components. *J. Biol. Chem.* 281:26391–26399.

Hill, M.M., M. Bastiani, R. Luetterforst, M. Kirkham, A. Kirkham, S.J. Nixon, P. Walser, D. Abankwa, V.M. Oorschot, S. Martin, et al. 2008. PTRF-Cavin, a conserved cytoplasmic protein required for caveola formation and function. *Cell.* 132:113–124.

Jin, S., and A.S. Verkman. 2007. Single particle tracking of complex diffusion in membranes: simulation and detection of barrier, raft, and interaction phenomena. *J. Phys. Chem. B.* 111:3625–3632.

Jin, S., P.M. Haggie, and A.S. Verkman. 2007. Single-particle tracking of membrane protein diffusion in a potential: simulation, detection, and application to confined diffusion of CFTR Cl- channels. *Biophys. J.* 93:1079–1088.

Jones, K.A., X. Jiang, Y. Yamamoto, and R.S. Yeung. 2004. Tuberin is a component of lipid rafts and mediates caveolin-1 localization: role of TSC2 in post-Golgi transport. *Exp. Cell Res.* 295:512–524.

Jordan, C., B. Puschel, R. Koob, and D. Drenckhahn. 1995. Identification of a binding motif for ankyrin on the alpha-subunit of Na+,K(+)-ATPase. *J. Biol. Chem.* 270:29971–29975.

Kaplan, J.H. 2002. Biochemistry of Na,K-ATPase. *Annu. Rev. Biochem.* 71:511–535.

Kasahara, K., Y. Nakayama, K. Ikeda, Y. Fukushima, D. Matsuda, S. Horimoto, and N. Yamaguchi. 2004. Trafficking of Lyn through the Golgi caveolin involves the charged residues on alphaE and alphaI helices in the kinase domain. *J. Cell Biol.* 165:641–652.

Kimura, T., P.B. Allen, A.C. Nairn, and M.J. Caplan. 2007. Arrestins and spinophilin competitively regulate Na+,K+-ATPase trafficking through association with a large cytoplasmic loop of the Na+,K+-ATPase. *Mol. Biol. Cell.* 18:4508–4518.

Le Lay, S., E. Hajduch, M.R. Lindsay, X. Le Liepvre, C. Thiele, P. Ferre, R.G. Parton, T. Kurzchalia, K. Simons, and I. Dugail. 2006. Cholesterol-induced caveolin targeting to lipid droplets in adipocytes: a role for caveolar endocytosis. *Traffic.* 7:549–561.

Leclerc, P.C., M. Auger-Messier, P.M. Lanctot, E. Escher, R. Leduc, and G. Guillemette. 2002. A polyaromatic caveolin-binding-like motif in the cytoplasmic tail of the type 1 receptor for angiotensin II plays an important role in receptor trafficking and signaling. *Endocrinology.* 143:4702–4710.

Liang, M., T. Cai, J. Tian, W. Qu, and Z.J. Xie. 2006. Functional characterization of Src-interacting Na/K-ATPase using RNA interference assay. *J. Biol. Chem.* 281:19709–19719.

Liang, M., J. Tian, L. Liu, S. Pierre, J. Liu, J. Shapiro, and Z.J. Xie. 2007. Identification of a pool of non-pumping Na/K-ATPase. *J. Biol. Chem.* 282:10585–10593.

Lingrel, J.B., and T. Kuntzweiler. 1994. Na+,K(+)-ATPase. *J. Biol. Chem.* 269:19659–19662.

Liu, J., R. Kesiry, S.M. Periyasamy, D. Malhotra, Z. Xie, and J.I. Shapiro. 2004. Ouabain induces endocytosis of plasmalemmal Na/K-ATPase in LLC-PK1 cells by a clathrin-dependent mechanism. *Kidney Int.* 66:227–241.

Liu, J., M. Liang, L. Liu, D. Malhotra, Z. Xie, and J.I. Shapiro. 2005. Ouabain-induced endocytosis of the plasmalemmal Na/K-ATPase in LLC-PK1 cells requires caveolin-1. *Kidney Int.* 67:1844–1854.

Liu, L., and A. Askari. 2006. Beta-subunit of cardiac Na+-K+-ATPase dictates the concentration of the functional enzyme in caveolae. *Am. J. Physiol. Cell Physiol.* 291:C569–C578.

Liu, L., K. Mohammadi, B. Aynafshar, H. Wang, D. Li, J. Liu, A.V. Ivanov, Z. Xie, and A. Askari. 2003. Role of caveolae in signal-transducing function of cardiac Na+/K+-ATPase. *Am. J. Physiol. Cell Physiol.* 284:C1550–C1560.

Liu, P., M. Rudick, and R.G. Anderson. 2002. Multiple functions of caveolin-1. *J. Biol. Chem.* 277:41295–41298.

Luetterforst, R., E. Stang, N. Zorzi, A. Carozzi, M. Way, and R.G. Parton. 1999. Molecular characterization of caveolin association with the Golgi complex: identification of a cis-Golgi targeting domain in the caveolin molecule. *J. Cell Biol.* 145:1443–1459.

Mayoral, R., A. Fernandez-Martinez, R. Roy, L. Bosca, and P. Martin-Sanz. 2007. Dispensability and dynamics of caveolin-1 during liver regeneration and in isolated hepatic cells. *Hepatology.* 46:813–822.

McCall, D. 1979. Cation exchange and glycoside binding in cultured rat heart cells. *Am. J. Physiol.* 236:C87–C95.

Morth, J.P., B.P. Pedersen, M.S. Toustrup-Jensen, T.L. Sorensen, J. Petersen, J.P. Andersen, B. Vilsen, and P. Nissen. 2007. Crystal structure of the sodium-potassium pump. *Nature.* 450:1043–1049.

Mundy, D.I., T. Machleidt, Y.S. Ying, R.G. Anderson, and G.S. Bloom. 2002. Dual control of caveolar membrane traffic by microtubules and the actin cytoskeleton. *J. Cell Sci.* 115:4327–4339.

Murata, M., J. Peranen, R. Schreiner, F. Wieland, T.V. Kurzchalia, and K. Simons. 1995. VIP21/caveolin is a cholesterol-binding protein. *Proc. Natl. Acad. Sci. USA.* 92:10339–10343.

Nguyen, A.N., D.P. Wallace, and G. Blanco. 2007. Ouabain binds with high affinity to the Na,K-ATPase in human polycystic kidney cells and induces extracellular signal-regulated kinase activation and cell proliferation. *J. Am. Soc. Nephrol.* 18:46–57.

Nichols, B.J. 2002. A distinct class of endosome mediates clathrin-independent endocytosis to the Golgi complex. *Nat. Cell Biol.* 4:374–378.

Nichols, B. 2003. Caveosomes and endocytosis of lipid rafts. *J. Cell Sci.* 116:4707–4714.

Nudelman, G., and Y. Louzoun. 2006. Cell surface dynamics: the balance between diffusion, aggregation and endocytosis. *Syst. Biol. (Stevenage).* 153:34–42.

Parton, R.G., and K. Simons. 2007. The multiple faces of caveolae. *Nat. Rev. Mol. Cell Biol.* 8:185–194.

Pelkmans, L., and A. Helenius. 2002. Endocytosis via caveolae. *Traffic.* 3:311–320.

Pelkmans, L., and M. Zerial. 2005. Kinase-regulated quantal assemblies and kiss-and-run recycling of caveolae. *Nature.* 436:128–133.

Pelkmans, L., J. Kartenbeck, and A. Helenius. 2001. Caveolar endocytosis of simian virus 40 reveals a new two-step vesicular-transport pathway to the ER. *Nat. Cell Biol.* 3:473–483.

Pelkmans, L., D. Puntener, and A. Helenius. 2002. Local actin polymerization and dynamin recruitment in SV40-induced internalization of caveolae. *Science.* 296:535–539.

Pol, A., S. Martin, M.A. Fernandez, M. Ingelmo-Torres, C. Ferguson, C. Enrich, and R.G. Parton. 2005. Cholesterol and fatty acids regulate dynamic caveolin trafficking through the Golgi complex and between the cell surface and lipid bodies. *Mol. Biol. Cell.* 16:2091–2105.

Qian, H., M.P. Sheetz, and E.L. Elson. 1991. Single particle tracking. Analysis of diffusion and flow in two-dimensional systems. *Biophys. J.* 60:910–921.

Rajasekaran, S.A., S.P. Barwe, and A.K. Rajasekaran. 2005. Multiple functions of Na,K-ATPase in epithelial cells. *Semin. Nephrol.* 25:328–334.

Razani, B., S.E. Woodman, and M.P. Lisanti. 2002. Caveolae: from cell biology to animal physiology. *Pharmacol. Rev.* 54:431–467.

Richter, T., M. Floetenmeyer, C. Ferguson, J. Galea, J. Goh, M.R. Lindsay, G.P. Morgan, B.J. Marsh, and R.G. Parton. 2008. High-resolution 3D quantitative analysis of caveolar ultrastrucutre and caveola-cytoskeleton interactions. *Traffic.* 9:893–909.

Rothberg, K.G., J.E. Heuser, W.C. Donzell, Y.S. Ying, J.R. Glenney, and R.G. Anderson. 1992. Caveolin, a protein component of caveolae membrane coats. *Cell.* 68:673–682.

Salanueva, I.J., A. Cerezo, M.C. Guadamillas, and M.A. del Pozo. 2007. Integrin regulation of caveolin function. *J. Cell. Mol. Med.* 11:969–980.

Sato, Y., I. Sagami, and T. Shimizu. 2004. Identification of caveolin-1-interacting sites in neuronal nitric-oxide synthase. Molecular mechanism for inhibition of NO formation. *J. Biol. Chem.* 279:8827–8836.

Saxton, M.J., and K. Jacobson. 1997. Single-particle tracking: applications to membrane dynamics. *Annu. Rev. Biophys. Biomol. Struct.* 26:373–399.

Schlegel, A., and M.P. Lisanti. 2000. A molecular dissection of caveolin-1 membrane attachment and oligomerization. Two separate regions of the caveolin-1 C-terminal domain mediate membrane binding and oligomer/oligomer interactions in vivo. *J. Biol. Chem.* 275:21605–21617.

Schlegel, A., R.G. Pestell, and M.P. Lisanti. 2000. Caveolins in cholesterol trafficking and signal transduction: implications for human disease. *Front. Biosci.* 5:D929–D937.

Sharma, D.K., J.C. Brown, A. Choudhury, T.E. Peterson, E. Holicky, D.L. Marks, R. Simari, R.G. Parton, and R.E. Pagano. 2004. Selective stimulation of caveolar endocytosis by glycosphingolipids and cholesterol. *Mol. Biol. Cell.* 15:3114–3122.

Song, K.S., S. Li, T. Okamoto, L.A. Quilliam, M. Sargiacomo, and M.P. Lisanti. 1996. Co-purification and direct interaction of Ras with caveolin, an integral membrane protein of caveolae microdomains. Detergent-free purification of caveolae microdomains. *J. Biol. Chem.* 271:9690–9697.

Souto, R.P., G. Vallega, J. Wharton, J. Vinten, J. Tranum-Jensen, and P.F. Pilch. 2003. Immunopurification and characterization of rat adipocyte caveolae suggest their dissociation from insulin signaling. *J. Biol. Chem.* 278:18321–18329.

Sweadner, K.J. 1989. Isozymes of the Na+/K+-ATPase. *Biochim. Biophys. Acta.* 988:185–220.

Tagawa, A., A. Mezzacasa, A. Hayer, A. Longatti, L. Pelkmans, and A. Helenius. 2005. Assembly and trafficking of caveolar domains in the cell: caveolae as stable, cargo-triggered, vesicular transporters. *J. Cell Biol.* 170:769–779.

Thomsen, P., K. Roepstorff, M. Stahlhut, and B. van Deurs. 2002. Caveolae are highly immobile plasma membrane microdomains, which are not involved in constitutive endocytic trafficking. *Mol. Biol. Cell.* 13:238–250.

Tian, J., T. Cai, Z. Yuan, H. Wang, L. Liu, M. Haas, E. Maksimova, X.Y. Huang, and Z.J. Xie. 2006. Binding of Src to Na+/K+-ATPase forms a functional signaling complex. *Mol. Biol. Cell.* 17:317–326.

Wang, H., M. Haas, M. Liang, T. Cai, J. Tian, S. Li, and Z. Xie. 2004. Ouabain assembles signaling cascades through the caveolar Na+/K+-ATPase. *J. Biol. Chem.* 279:17250–17259.

Wang, Y., K. Yamaguchi, T. Wada, K. Hata, X. Zhao, T. Fujimoto, and T. Miyagi. 2002. A close association of the ganglioside-specific sialidase Neu3 with caveolin in membrane microdomains. *J. Biol. Chem.* 277:26252–26259.

Williams, T.M., and M.P. Lisanti. 2004. The Caveolin genes: from cell biology to medicine. *Ann. Med.* 36:584–595.

Wu, M., J. Fan, W. Gunning, and M. Ratnam. 1997. Clustering of GPI-anchored folate receptor independent of both cross-linking and association with caveolin. *J. Membr. Biol.* 159:137–147.

Xie, Z., and T. Cai. 2003. Na+-K+–ATPase-mediated signal transduction: from protein interaction to cellular function. *Mol. Interv.* 3:157–168.

Yuan, Z., T. Cai, J. Tian, A.V. Ivanov, D.R. Giovannucci, and Z. Xie. 2005. Na/K-ATPase tethers phospholipase C and IP3 receptor into a calcium-regulatory complex. *Mol. Biol. Cell.* 16:4034–4045.